

# Multi-omics Investigation into the Mechanism of Action of an Anti-tubercular Fatty Acid Analogue

Isin T. Sakallioğlu, Amith S. Maroli, Aline De Lima Leite, Darrell D. Marshall, Boone W. Evans, Denise K. Zinniel, Patrick H. Dussault, Raúl G. Barletta, and Robert Powers\*



Cite This: *J. Am. Chem. Soc.* 2022, 144, 21157–21173



Read Online

ACCESS |



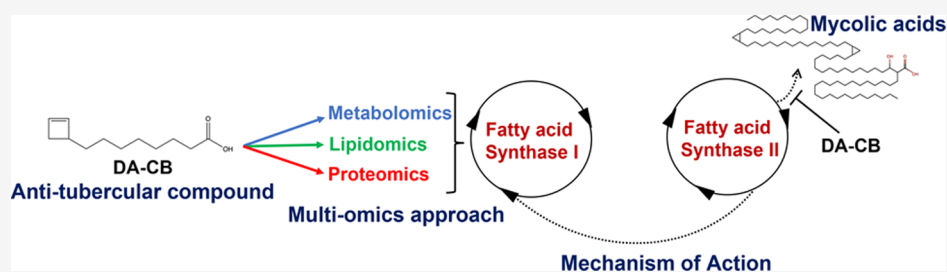
Metrics & More



Article Recommendations



Supporting Information



**ABSTRACT:** The mechanism of action (MoA) of a clickable fatty acid analogue 8-(2-cyclobuten-1-yl)octanoic acid (DA-CB) has been investigated for the first time. Proteomics, metabolomics, and lipidomics were combined with a network analysis to investigate the MoA of DA-CB against *Mycobacterium smegmatis* (*Msm*). The metabolomics results showed that DA-CB has a general MoA related to that of ethionamide (ETH), a mycolic acid inhibitor that targets enoyl-ACP reductase (InhA), but DA-CB likely inhibits a step downstream from InhA. Our combined multi-omics approach showed that DA-CB appears to disrupt the pathway leading to the biosynthesis of mycolic acids, an essential mycobacterial fatty acid for both *Msm* and *Mycobacterium tuberculosis* (*Mtb*). DA-CB decreased keto-meromycolic acid biosynthesis. This intermediate is essential in the formation of mature mycolic acid, which is a key component of the mycobacterial cell wall in a process that is catalyzed by the essential polyketide synthase Pks13 and the associated ligase FadD32. The multi-omics analysis revealed further collateral alterations in bacterial metabolism, including the overproduction of shorter carbon chain hydroxy fatty acids and branched chain fatty acids, alterations in pyrimidine metabolism, and a predominate downregulation of proteins involved in fatty acid biosynthesis. Overall, the results with DA-CB suggest the exploration of this and related compounds as a new class of tuberculosis (TB) therapeutics. Furthermore, the clickable nature of DA-CB may be leveraged to trace the cellular fate of the modified fatty acid or any derived metabolite or biosynthetic intermediate.

## INTRODUCTION

Tuberculosis (TB) is a disease caused by *Mycobacterium tuberculosis* (*Mtb*).<sup>1</sup> In 2021, over 10 million new cases of TB were reported worldwide.<sup>2</sup> Currently, TB treatment is a slow and tedious regimen, in which multiple drugs are prescribed over the course of many months.<sup>3–9</sup> Moreover, non-compliance with the treatment schedule has led to the reemergence of TB in the form of both multi-drug-resistant and extensive drug-resistant (i.e., MDR/XDR-TB) strains.<sup>10–13</sup> In the quest to keep pace with TB antibiotic resistance, drug discovery efforts have emphasized the identification of new drug candidates that operate by novel mechanisms of action (MoA).<sup>14</sup> In this regard, we previously synthesized and investigated 11 fatty acid analogues, 6 of which showed minimum inhibitory concentration (MIC) values equivalent to or better than the second-line TB drug D-cycloserine (DCS).<sup>15,16</sup> The fatty acid motifs were based on frameworks derived from decanoic acid (C<sub>10</sub>), oleic acid, or elaidic acid (both C<sub>18</sub>). Several of these fatty acid analogues displayed low micromolar MIC values against various *Mtb* strains, where 8-

(2-cyclobuten-1-yl)octanoic acid (DA-CB), a cyclobutene-containing analogue of decanoic acid, exhibited activity similar to that of the TB drugs, isoniazid (INH) and ethionamide (ETH). In addition to its efficacy, DA-CB is an intriguing lead compound because a strained cyclic alkene is present. This feature enables selective addressing of DA-CB or any derived biosynthetic intermediate via a “click” reaction,<sup>17–20</sup> providing a handle with which to decipher the location of the fatty acid analogue or derived conjugates within the mycobacterial cell.

The versatility and pathogenicity of mycobacteria are primarily due to the make-up of the cellular envelope and their ability to survive and replicate intracellularly.<sup>1</sup> The thick cell wall provides a protective layer against a host’s immune

Received: August 3, 2022

Published: November 11, 2022



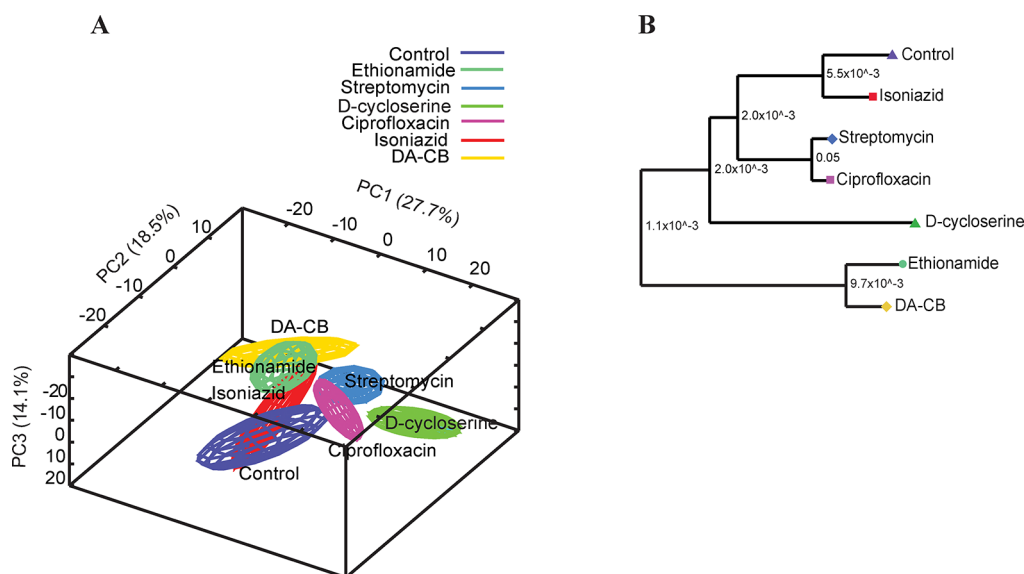


**Figure 1.** (A) PCA score plot generated from 1D  $^1\text{H}$  NMR data set using MVAPACK with three principal components. The PCA plot exhibits group differentiation with  $R^2 = 0.755$  and  $Q^2 = 0.640$ . Untargeted metabolomics of *Msm* cells (purple), cells treated with isoniazid (INH, red), D-cycloserine (DCS, dark green), ethionamide (ETH, green), ciprofloxacin (magenta), streptomycin (blue), and DA-CB (yellow). Ellipsoids represent a 95% confidence limit of the normal distribution of each cluster. (B) Dendrogram generated from the PCA score plot with each Mahalanobis distance  $p$ -value represented between the nodes shows DA-CB is closely clustered with ethionamide.

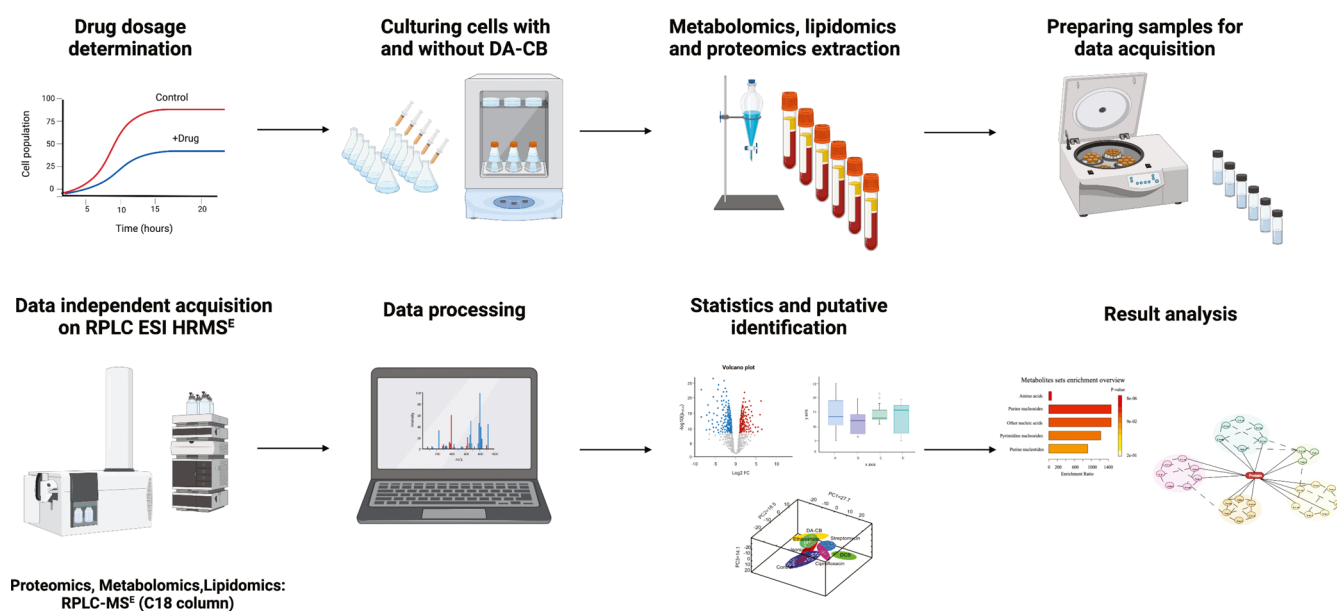
system, assists with antibacterial resistance, and increases structural integrity.<sup>21–24</sup> The cell wall structure also differentiates mycobacteria from other prokaryotes. Accordingly, drug candidates that target mycobacterial cell wall biosynthesis are highly desirable.<sup>22,23</sup> Indeed, the most commonly used TB drug treatments, INH and ETH, target the biosynthesis of mycolic acids, structurally distinct fatty acids unique to mycobacteria.<sup>25–28</sup> These compounds differ from common fatty acids in their size (60–90 carbons), the presence of two major branches, and the frequent fusion of cyclopropanes onto the backbone. The biosynthesis of mycolic acids begins with the formation of malonyl-CoA and acetyl-CoA, which are further elongated by fatty acid synthetase type I (FAS-I). Incorporation of double bonds is mediated by the activation of desaturases and fatty acid type II synthetases (FAS-II). The introduction of cyclopropanes by cyclopropane synthetase forms alpha-meroacyl-ACP, the source of alpha-mycolic acid.<sup>29</sup> Both *Mycobacterium smegmatis* (*Msm*) and *Mtb* can readily take-up fatty acids and convert them into mycolic acids.<sup>27,28</sup> Morbidoni et al. (2012) discovered two unnatural fatty acids containing carbon–carbon triple bonds, 2-hexadecynoic acid and 2-octadecynoic acid, that are active against *Msm*.<sup>30</sup> The modified fatty acids or derived species might destabilize the organism by inhibiting the mycolic acid biosynthetic machinery or by changing the integrity of the cell wall.<sup>15,30</sup> At the outset of these studies, we hypothesized that DA-CB might well function through a similar mechanism.

Proteomics is a valuable tool for identifying potential drug candidates while also providing an initial understanding of drug target interactions.<sup>31</sup> Similarly, metabolomics has shown enormous potential when applied to investigating drug mechanisms, disease processes, and drug discovery.<sup>32,33</sup> In this regard, metabolomics has been used for rapidly elucidating the MoA of novel drug candidates.<sup>34–37</sup> A specialized subdivision of metabolomics, lipidomics has also been used to elucidate the MoA of drugs; the broadened coverage of biological pathways offered by lipidomics is of utmost

importance to determine potential alterations in the lipid-rich mycobacterial cell wall.<sup>38,39</sup> An example can be seen in the recent use of lipidomics to elucidate the MoA for the anti-trypansomal drug miltefosine.<sup>40</sup> The drug was a priori predicted to be affecting phospholipid metabolism due to its lipid-similar structure, and lipidomics studies revealed that miltefosine produces major alterations in phospholipid levels. Simultaneously integrating lipidomics, metabolomics, and proteomics is expected to improve the efficiency and accuracy of MoA elucidation while also enhancing our understanding of the overall biological response to an individual drug treatment.<sup>41,42</sup> Simply, a multi-omics approach is capable of measuring changes across a larger and more diverse set of biomolecules, while providing a more complete and system-wide picture of drug-induced cellular changes.<sup>43</sup> This wider span of coverage enables the construction of a unified and consensus network that permits the identification of off-target or secondary perturbations that commonly confound the analysis of omics data sets.<sup>42,44</sup> A resulting network generated from a combined proteomics, lipidomics, and metabolomics data set facilitates the analysis of drug activities by enabling the construction of predictive models of therapeutic efficacy and the identification of the lethal protein target(s) — the cellular target of a drug whose inhibition directly leads to cell death.

Herein, we describe an investigation into the MoA of DA-CB against *Msm* using a multi-omics approach that includes proteomics, metabolomics, and lipidomics. DA-CB appears to disrupt the pathway leading to the biosynthesis of mycolic acids, an essential mycobacterial fatty acid for both *Msm* and *Mtb*. Our results suggest that DA-CB and related molecules have the potential for development as TB therapeutics. Moreover, the clickable nature of DA-CB may be leveraged to trace the cellular fate of the modified fatty acid or any derived synthetic intermediate.<sup>20</sup>

**Scheme 1. Workflow of Multi-omics Sample Preparation and Data Acquisition Using Reversed-Phase Liquid Chromatography Electrospray Ionization High-Resolution Mass Spectrometry (RPLC ESI HRMS<sup>E</sup>) from DA-CB-Treated *Msm*. Created with BioRender.com**



## RESULTS AND DISCUSSION

**DA-CB Has a Similar MoA as ETH, a Mycolic Acid Inhibitor.** Compounds with a fatty acid skeleton, including some functionalized synthetic analogues of natural fats, can be incorporated into fatty acid biosynthetic pathways.<sup>30</sup> The fatty acid analogue of interest, DA-CB, has a MIC value for *Mtb* strains lower than 100  $\mu\text{M}$ . This is similar to known inhibitors of cell wall biosynthesis (e.g., DCS and INH) used to treat *Mtb* infections. We have hypothesized that the *Msm* and *Mtb* inhibition observed with DA-CB may result from interference with cell wall biosynthesis or by alterations in the properties of the cell wall following incorporation of the modified fatty acid.

Our investigation into the MoA for DA-CB began with a comparison of the metabolic fingerprints of *Msm* after treatment with DA-CB or other anti-tubercular drugs with a known MoA, including known inhibitors of mycolic acid synthesis. The specific anti-tubercular drugs used in the metabolic fingerprint comparison included ciprofloxacin that inhibits DNA gyrase and prevents DNA supercoiling; DCS that prevents peptidoglycan biosynthesis; ETH and INH that both disrupt mycolic acid formation by inhibiting the enoyl-ACP reductase (InhA); and streptomycin that inhibits protein synthesis by binding to the 30S ribosomal protein S12 and 16S rRNA.<sup>36</sup> To analyze these effects for DA-CB, we determined the concentration of DA-CB that inhibited growth by 50% (i.e., a sublethal drug dosage) under conditions equivalent to our metabolomics studies and as previously described.<sup>36</sup> After these drug treatments, the *Msm* cells were lysed, and the cellular metabolome extract was analyzed by NMR. Metabolic fingerprints obtained from one-dimensional (1D) <sup>1</sup>H NMR data sets have been frequently employed to predict the general *in vivo* MoA for drug leads.<sup>35,37</sup> Drugs with similar MoAs would be expected to induce similar metabolic fingerprints and would cluster together in the score plot from principal components analysis (PCA). The PCA score plot followed by a hierarchical clustering analysis showed a close relationship

between the DA-CB and ETH-induced *Msm* metabolomes (Figure 1).

An OPLS model comparing only the DA-CB-treated or untreated *Msm* metabolomes (Figure S1A) was used to create a back-scaled loading plot (Figure S1B) to identify the key metabolites that differentiated between the two groups. Specifically, glutamate was significantly decreased in DA-CB-treated cells while alanine, AMP, glucose-1-phosphate, lactate, trehalose, and valine were increased. A follow-up two-dimensional (2D) <sup>1</sup>H–<sup>13</sup>C heteronuclear single-quantum coherence (HSQC) analysis of the <sup>13</sup>C-carbon-labeled *Msm* metabolomes identified over 40 metabolites derived from <sup>13</sup>C-glucose that were significantly altered (false discover rate (FDR)-corrected *p*-value < 0.05) due to a DA-CB treatment. A heatmap (Figure S2A) and network map (Figure S2B) summarize these results. Overall, the preliminary NMR metabolomics analysis suggests that DA-CB causes an increase in glycolysis and fatty acid metabolism and a reduction in arginine and pyrimidine metabolism.

ETH is a second-line drug commonly used to treat TB. ETH is structurally similar to INH, and both are inhibitors of mycolic acid biosynthesis. Although they are both pro-drugs, the pathway of activation for ETH is distinct from INH.<sup>45</sup> Specifically, ETH is activated by the mono-oxygenase EthA. In contrast, INH is activated by the peroxidase KatG. Both enzymes form a stable covalent adduct with nicotinamide adenine dinucleotide (NAD)<sup>46</sup> that inhibits InhA, which is involved in mycolic acid biosynthesis.<sup>37,45,47,48</sup>

As DA-CB may also inhibit mycolic acid biosynthesis, we investigated the cellular processes that DA-CB alters by employing a multi-omics approach to characterize the metabolome, proteome, and lipidome of *Msm*. Statistical analysis of these individual omics data sets showed a significant alteration due to DA-CB. *Msm* cells were treated with DA-CB or DMSO (as a control) and lysed, and the metabolome, lipidome, and proteome were extracted for reversed-phase ultra-high-pressure liquid chromatography mass spectrometry in a data-independent acquisition mode (RP UHPLC-DIA-

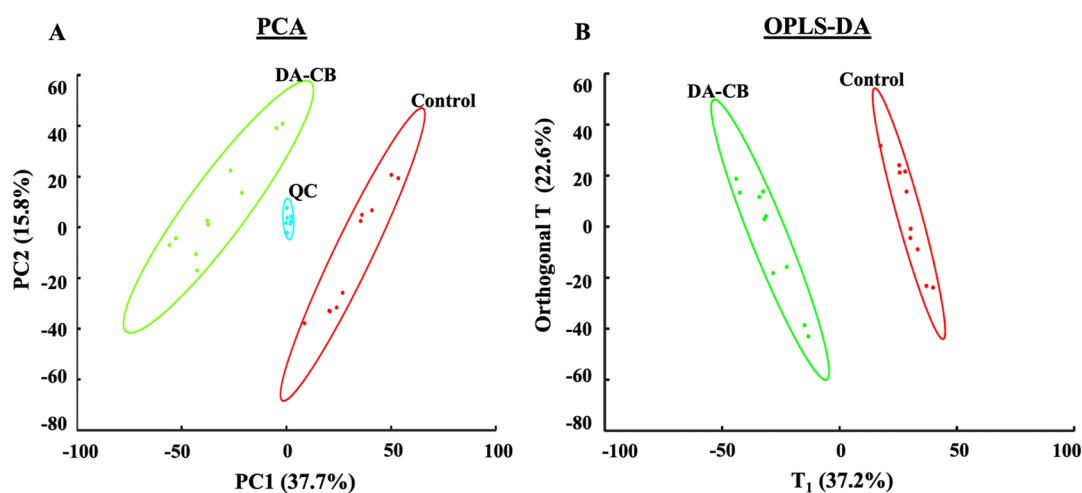


**Figure 2.** (A) PCA ( $R^2 = 0.535$  and  $Q^2 = 0.391$ ) with five principal components and (B) orthogonal projection to latent structures discriminant analysis (OPLS-DA,  $R^2 = 0.990$ ,  $Q^2 = 0.959$ , and  $p$ -value  $< 0.03$ ) models generated from the LC–MS metabolomics data set. *Msm* cells were treated with either 400  $\mu\text{M}$  of DA-CB (green) or 10  $\mu\text{L}$  of DMSO (control, red). Quality control (QC) pooled samples combine 45  $\mu\text{L}$  from each DA-CB and control sample. Ellipses represent a 95% confidence limit of the normal distribution of each cluster.

MS). The RP UHPLC-DIA-MS lipidomics data acquisition protocol was previously optimized to ensure complete coverage of the mycobacterial lipidome, with a special emphasis in the detection of mycolic acids.<sup>49</sup> The lipidomics and metabolomics data were processed and analyzed with statistical software packages.<sup>50</sup> The multi-omics protocol employed to characterize the cellular impact of DA-CB is summarized in Scheme 1.<sup>51</sup>

**Metabolomics-Identified Amino Acids, Purines, Pyrimidines, and Fatty Acyl Glycosides Were Altered by DA-CB.** The liquid chromatography–mass spectrometry (LC–MS) metabolomics data yielded 8,074 spectral features. The resulting unsupervised PCA model yielded a clear separation between the control and DA-CB treatment groups in the score plot (Figure 2A). The tight clustering of the quality control samples in the center of the score plot is significant, testifying to the high quality of the metabolomics data set. A supervised OPLS model (Figure 2B) yielded a similar level of group separation and identified features or metabolites that differentiated the two groups. The OPLS model was validated using a permutation test ( $n = 1000$ ,  $p$ -value  $< 0.03$ ) and determined to be of high quality, given the  $R^2$  (0.990) and  $Q^2$  (0.959) values (Table S1). Overall, the PCA and OPLS models of the LC–MS metabolomics data set clearly demonstrate statistically significant DA-CB-induced perturbations in the global cellular metabolome of *Msm*.

The entire LC–MS data set was curated to only include features with statistically significant group differences to identify metabolic pathways potentially affected by DA-CB. A total of 180 LC–MS features were deemed statistically significant based on a VIP score  $> 1.0$ , an FDR-corrected  $p$ -value  $< 0.05$ , and a fold change  $> 1.5$ . The exact mass, isotopic pattern, and fragmentation pattern for these 180 features were submitted to Progenesis Q1 metabolomics software to identify 26 putative metabolites altered by DA-CB (Table 1). An enrichment analysis with MetaboAnalyst revealed that the top five metabolic pathway changes were related to amino acids, purine nucleosides, other nucleic acids, pyrimidine nucleosides, and purine nucleotides (Figure 3A). Box plots summarizing the relative concentration changes for the metabolites associated with these pathways are shown in Figure 3B–G. The DA-CB

treatment resulted in a general increase in the concentration of acyl-CoA, amino acids, dipeptides, and purines. Conversely, concentrations of uridine-diphosphate, methylthioadenosine, and deoxyguanosine monophosphate were significantly decreased. Encouragingly, the preliminary NMR metabolomics analysis was also consistent with and support these LC–MS metabolomics outcomes. NMR and MS metabolomics analyses of the same biological samples detect distinct sets of metabolites that have been previously shown to provide complementary information.<sup>52</sup>

**Lipidomics-Identified DA-CB-Associated Alteration of Wax Monoesters, Branched Chain Fatty Acids, and Mycolic Acids.** We characterized the lipidome changes to further explore the impact of DA-CB on *Msm* metabolism, especially given the predicted relationship between DA-CB and the mycolic acid inhibitor ETH. We employed our previously described LC–MS lipidomics protocol to maximize the coverage of the *Msm* lipidome to include mycolic acids.<sup>49</sup> The same cellular extract samples were used for both the metabolomics and lipidomics experiments. The LC–MS data set was collected in both negative and positive ionization modes, which yielded 6,033 and 5,281 spectral features, respectively. Separate PCA and OPLS models were created from the two LC–MS lipidomics data sets to maximize the identification of all the lipids altered by DA-CB and to obtain a complete picture of the impact of DA-CB on *Msm*. Simply, we expected and observed different sets of lipids detected in the negative and positive ionization modes. Combining both data sets into a single statistical model would likely emphasize the highly altered lipids with the potential loss of moderately changing lipids, which was not advantageous. Both PCA models showed a clear separation between the DA-CB treatment and control groups and were statistically significant as evident by average  $R^2$  and  $Q^2$  values of 0.745 and 0.644, respectively (Figure 4, Table S1). Similarly, the OPLS models were statistically valid as assessed by  $p$ -values  $< 0.01$  from a permutation test ( $n = 1000$ ) and were of high quality based on average  $R^2$  and  $Q^2$  values of 0.992 and 0.980, respectively (Figure 4B, D and Table S1).

The lipidomics data set was key to the overall analysis of the metabolic impact of DA-CB and its comparison to ETH.

Table 1. Metabolites Significantly Altered by DA-CB Treatment

pathway	class	subclass/direct parent	accepted description	VIP <sup>a</sup> OPLS	p-value <sup>b</sup>	FDR-corrected p-value <sup>c</sup>	FC <sup>d</sup>	
pyrimidine metabolism	pyrimidine nucleotide	pyrimidine nucleotide sugars	UDP-GlcNAc	1.44	$3.04 \times 10^{-7}$	$6.74 \times 10^{-7}$	0.49	
	pyrimidine nucleotide	pyrimidine ribonucleoside	uridine-diphosphate	1.29	$6.91 \times 10^{-6}$	$9.31 \times 10^{-6}$	0.62	
	organoxygen compounds	carbohydrates and conjugates/acyl amino sugars	beta-mannose-acylglucosamine	1.56	$1.55 \times 10^{-5}$	$2.00 \times 10^{-5}$	10.48	
	pyrimidine nucleotide	pyrimidine nucleotide sugars/same	deoxythymidine diphosphate-L-rhamnose	1.31	$1.05 \times 10^{-6}$	$1.72 \times 10^{-6}$	0.59	
amino acid metabolism	carboxylic acids and derivatives	amino acids, peptides/amino acids	ornithine	1.47	$1.23 \times 10^{-10}$	$5.43 \times 10^{-10}$	4.91	
		amino acids, peptides/dipeptides	acetyl-arginine	1.59	$1.42 \times 10^{-11}$	$1.08 \times 10^{-10}$	6.82	
	amino acids, peptides, and analogues/glutamine and derivatives	amino acids, peptides, and analogues/N-acyl-L-alpha-amino acids	glutamylglutamic acid	1.27	$3.25 \times 10^{-5}$	$3.73 \times 10^{-5}$	0.61	
		amino acids, peptides, and analogues/glutamine and derivatives	glutamyltryptophan	1.59	$5.53 \times 10^{-7}$	$9.84 \times 10^{-7}$	2.45	
		amino acids, peptides, and analogues/glutamine and derivatives	hydroxyprolyl-tyrosine	1.43	$3.27 \times 10^{-6}$	$4.61 \times 10^{-6}$	1.85	
		amino acids, peptides, and analogues/glutamine and derivatives	tyrosyl-hydroxyproline	1.61	$1.86 \times 10^{-11}$	$1.08 \times 10^{-10}$	0.19	
		amino acids, peptides, and analogues/glutamine and derivatives	hydroxyprolyl-proline	1.52	$2.24 \times 10^{-5}$	$2.68 \times 10^{-5}$	4.81	
	glycosylphosphatidylinositol (GPI)-anchor biosynthesis	amino acids, peptides, and analogues/glutamine and derivatives	hydroxyglutamine	1.58	$1.21 \times 10^{-6}$	$1.88 \times 10^{-6}$	0.66	
		amino acids, peptides, and analogues/glutamine and derivatives	succinyl-diaminopimelate	1.47	$5.71 \times 10^{-7}$	$9.84 \times 10^{-7}$	0.56	
	lipid metabolism	organoxygen compounds	amino acids, peptides, and analogues/N-acyl-L-alpha-amino acids	alpha-glucosaminyl-myo-inositol	1.58	$5.83 \times 10^{-8}$	$1.51 \times 10^{-7}$	6.43
		glycerophospholipid	carbohydrates and conjugates/aminocyclitol glycosides	LysoPE (0:0,20:4)	1.62	$1.07 \times 10^{-11}$	$1.08 \times 10^{-10}$	7.36
	oxidation of fatty acids	fatty acyls	glycerophosphoethanolamine	hydroxyoctanoyl carnitine	1.57	$2.16 \times 10^{-3}$	$2.23 \times 10^{-3}$	35.24
		fatty acyls	fatty acid esters	linoleoyl-CoA	1.60	$2.09 \times 10^{-11}$	$1.08 \times 10^{-10}$	7.79
pantothenate and CoA biosynthesis	organoxygen compounds	fatty acyl thioester/long chain fatty acyl-coa	pantothenic acid	1.48	$1.66 \times 10^{-6}$	$2.45 \times 10^{-6}$	0.44	
	organoxygen compounds	alcohols/secondary alcohols		1.48	$1.66 \times 10^{-6}$	$2.45 \times 10^{-6}$	0.44	
purine metabolism	purine nucleosides	purine deoxyribonucleosides	deoxyguanosine	1.51	$2.17 \times 10^{-8}$	$6.12 \times 10^{-8}$	0.58	
		cyclic purine nucleotides	cyclic AMP	1.20	$9.41 \times 10^{-8}$	$2.24 \times 10^{-7}$	1.73	
	purine nucleotide	purine nucleotide sugars	NADHX	1.61	$5.79 \times 10^{-14}$	$1.51 \times 10^{-12}$	0.25	
		purine deoxyribonucleotides	deoxyguanosine-monophosphate	1.30	$2.17 \times 10^{-8}$	$6.12 \times 10^{-8}$	2.23	
	dinucleotides	dinucleotides/dinucleotides	diadenosine diphosphate	1.62	$9.75 \times 10^{-14}$	$1.51 \times 10^{-12}$	244.79	
		carbohydrates and conjugates/pentose phosphates	inosine-phosphate	1.27	$5.82 \times 10^{-4}$	$6.23 \times 10^{-4}$	2.09	
	deoxyribonucleosides	purine ribonucleosides/deoxy-thionucleosides	methylthioadenosine	1.59	$6.38 \times 10^{-10}$	$2.47 \times 10^{-9}$	0.26	
		alloxazines/flavins	riboflavin	1.34	$2.95 \times 10^{-4}$	$3.27 \times 10^{-4}$	0.57	

<sup>a</sup>VIP score—variable importance in projection score from the OPLS-DA model. <sup>b</sup>p-value—Student's *t*-test *p*-value. <sup>c</sup>FDR-corrected *p*-value using the Benjamini–Hochberg method. <sup>d</sup>FC—fold change calculated using the average of the integrated peak area from DA-CB treatments divided by the average of the integrated peak area from control samples.

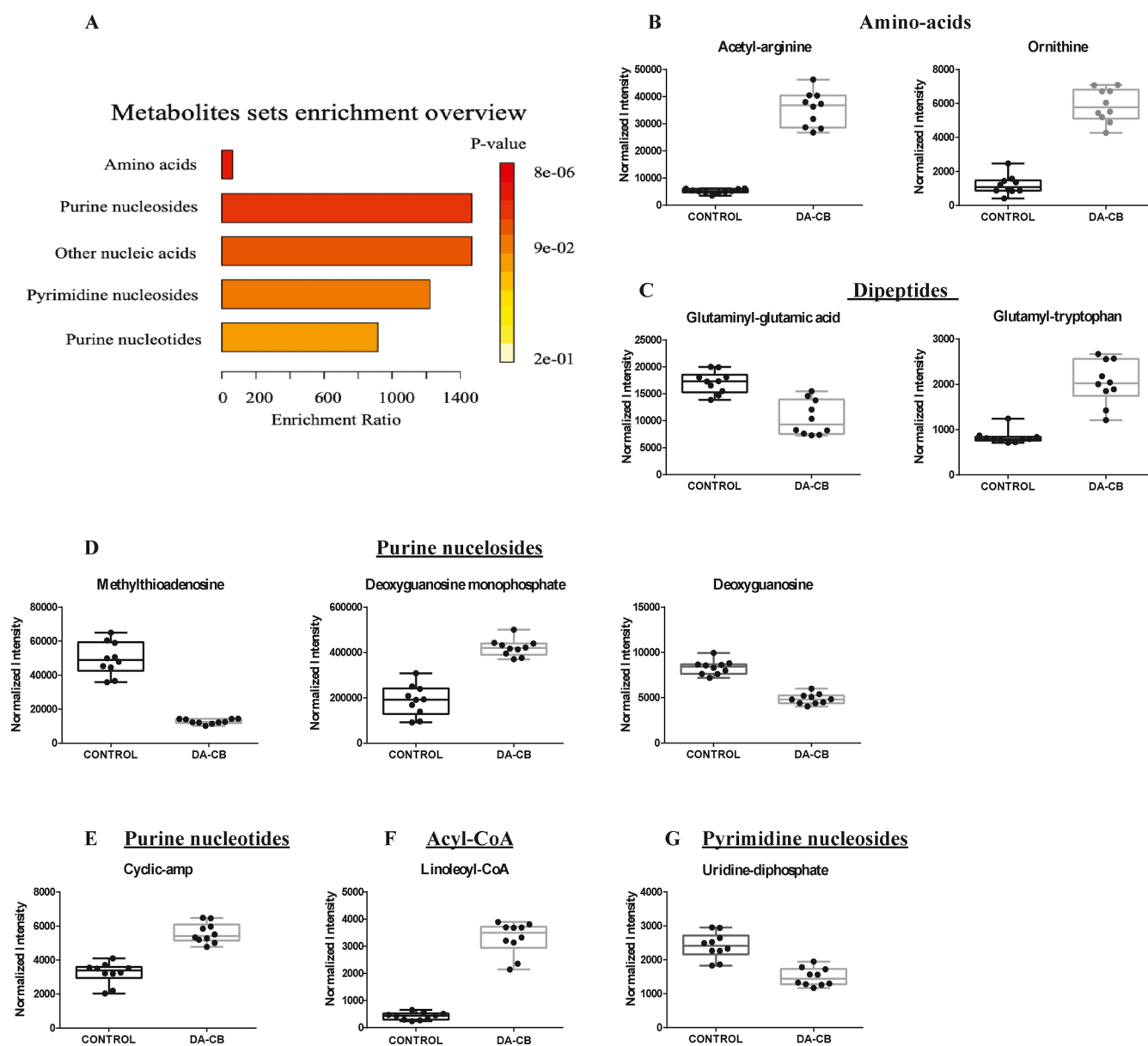


**Figure 3.** (A) Enrichment analysis using the 26 metabolites with statistically significant changes in *Msm* cells following DA-CB treatment. Representative box plots for significantly altered metabolites corresponding to the following enriched pathways: (B) amino acids, (C) dipeptides, (D) purine nucleosides, (E) purine nucleotides, (F) acyl-CoA, and (G) pyrimidine nucleosides. DA-CB indicates DA-CB-treated *Msm* cells and control indicates only DMSO-treated *Msm* cells.

Overall, the PCA and OPLS models for the lipidomics data sets demonstrated a significant DA-CB-induced perturbations in the global cellular lipidome relative to the controls. The LC-MS features with VIP scores  $\geq 1.0$ , FDR  $p$ -values  $< 0.05$ , and a fold change  $> 1.5$  were selected to identify the key lipids that differentiated between the two groups. A total of 170 positive mode spectral features and 133 negative mode spectral features incurred a statistically significant change due to DA-CB. The exact mass, isotopic pattern, and fragmentation pattern for these selected features were submitted to Progenesis Q1 metabolomics software to identify a total of 48 lipids. An enrichment analysis with MetaboAnalyst revealed that the top six ( $p$ -value  $< 0.001$ ) lipidomic pathways, indicated with the lipid classification names, were associated with wax monoesters, branched chain fatty acids, mycolic acids, and hydroxy, saturated, and unsaturated fatty acids (Figure 5A

and Table 2). The representative lipid box plots summarizing the relative concentration changes for the lipids associated with these pathways are shown in Figure 5B–G. The nine wax monoesters (lipid subclass) increased substantially relative to the control following DA-CB treatment (Figure 5B). Similarly, the six branched fatty acids (Figure 5C) and the saturated (Figure 5F) and unsaturated fatty acids (Figure 5G) all increased because of DA-CB. Conversely, the four mycolic acids (keto-meromycolic acid [ $C_{81}$ ], alpha-mycolic acid [ $C_{80}$ ], 2-eicosyl-3-hydroxy-32-oxo-33-methyl-nonatetracontanoic acid [ $C_{70}$ ], and corynomycolic acid [ $C_{32}$ ], Figure 5D) and the hydroxy fatty acids (Figure 5E) decreased significantly compared to controls following DA-CB treatment. While the preliminary NMR metabolomics data set was limited to aqueous metabolites, changes in precursor metabolites and water-soluble fatty acids still indicated a general increase in

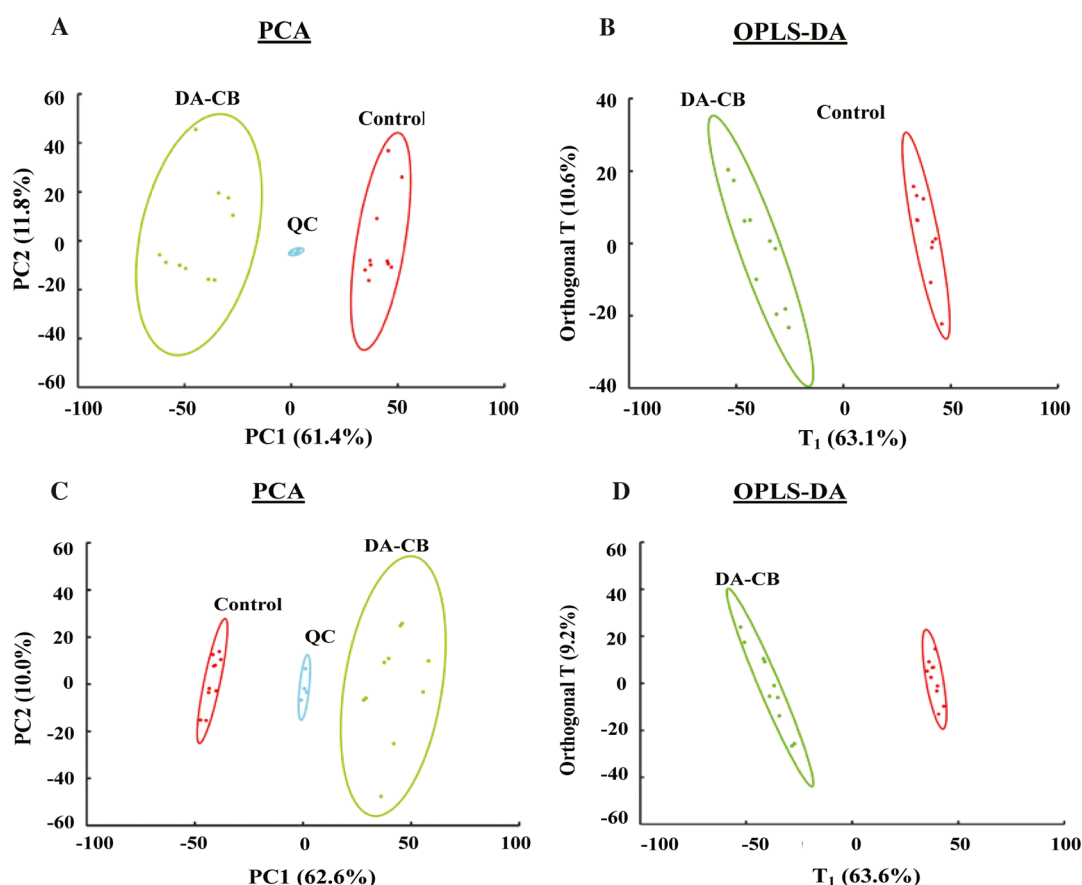


**Figure 4.** (A) PCA ( $R^2 = 0.745$ ,  $Q^2 = 0.644$ ) with five principal components and (B) orthogonal projection to latent structure discriminant analysis (OPLS-DA,  $R^2 = 0.992$ ,  $Q^2 = 0.980$ , and  $p$ -value  $< 0.01$ ) models generated from the positive ionization mode LC-MS lipidomics data set. (C) PCA ( $R^2 = 0.726$  and  $Q^2 = 0.613$ ) and (D) OPLS-DA ( $R^2 = 0.996$ ,  $Q^2 = 0.984$ , and  $p$ -value  $< 0.01$ ) models generated from the negative ionization mode LC-MS lipidomics data set. *Msm* cells were treated with either 400  $\mu\text{M}$  of DA-CB (green) or 10  $\mu\text{L}$  of DMSO (control, red). QC pooled samples combine 45  $\mu\text{L}$  from each DA-CB and control sample. Ellipses represent a 95% confidence limit of the normal distribution of each cluster.

branched chain fatty acids due to DA-CB treatment consistent with these findings from the LC-MS lipidomics results.

#### Proteomics Identified the Pentose Phosphate Pathway, the Biosynthesis of Unsaturated Fatty Acids, and Pyrimidine Metabolism as Being Altered by DA-CB.

A total of 858 proteins were detected with at least one unique peptide and a 1% FDR from a label-free untargeted LC-MS proteomic profiling of *Msm* following DA-CB treatment. A volcano plot for all the detected proteins is displayed in Figure S3. Curation of the proteomics data set for significant changes due to DA-CB identified 123 differentially expressed proteins with fold change  $> 1.2$  and  $p$ -value  $< 0.05$ , which included 53 proteins with an FDR-corrected  $p$ -value  $< 0.05$  (Table S2). The expression of 107 proteins decreased while that of 16 proteins increased due to the DA-CB treatment. A string network of the differentially expressed proteins is displayed in Figure S4. Interestingly, the upregulated proteins were primarily associated with three pathways: alpha-linolenic acid metabolism, geraniol degradation, and monobactam biosynthesis. The downregulated proteins were mainly associated with four pathways: pentose phosphate metabolism, biosynthesis of unsaturated fatty acids, pyrimidine metabolism, and alteration of ribosomal proteins. Importantly, a proteomic profile identifies only the relative change in the expression level of a protein and not a change in the activity of the protein. While an up- or downregulation may suggest a corresponding change in activity, the only definitive finding is a perturbation

in the pathway in response to DA-CB. While it is also tempting to interpret a correlated change between a protein and its metabolite/lipid substrate as a change in protein activity, there is still no direct experimental evidence that such an alteration has occurred.

A biological process enrichment network map was created using the 123 proteins with significantly altered expression levels to understand the key metabolic pathways effected by DA-CB (Figure 6A). The statistically significant ( $p$ -value  $< 0.05$ ) Genome Ontology-Kyoto Encyclopedia of Genes and Genomes (GO-KEGG) term clusters included proteins from the ribosome, pentose phosphate pathway (PPP), biosynthesis of unsaturated fatty acids, and pyrimidine metabolism (Figure 6B). The enriched biological processes (Figure 6C) also agreed with the significant alterations ( $p$ -value  $< 0.05$ ) in pyrimidine and pyridine biosynthesis, pentose phosphate shunt, and fatty acid metabolism. Furthermore, the genes corresponding to the enriched GO-KEGG pathways were identified. The metabolic pathways that were also enriched in the metabolomics and lipidomics data sets are shown in bold in Table 3. The altered metabolic pathways implicated by all the three omics data sets are as follows: PPP, pyrimidine metabolism, amino acid transport, biosynthesis of unsaturated fatty acids,  $\alpha$ -linolenic acid metabolism, fatty acid metabolism, biosynthesis of amino acids, and pantothenate and coenzyme A (CoA) biosynthesis. The proteins associated with PPP, pyrimidine metabolism, and the biosynthesis of amino acids

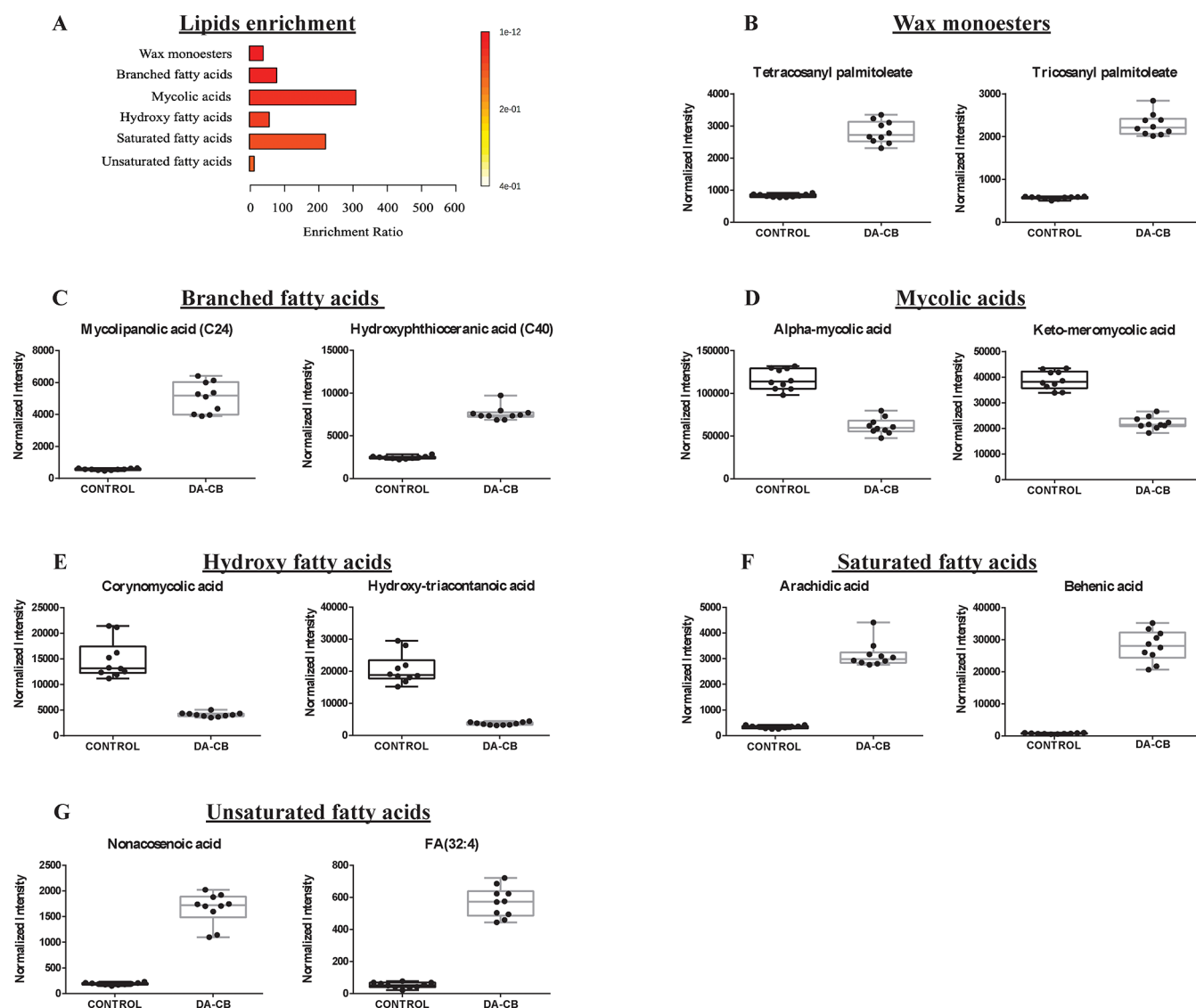


**Figure 5.** (A) Enrichment analysis using the 48 lipids with statistically significant changes in *Msm* cells following a DA-CB treatment. (B–G) Representative box plots for significantly altered lipids corresponding to the following enriched pathways: (B) wax monoesters, (C) branched chain fatty acids, (D) mycolic acids, (E) hydroxy fatty acids, (F) saturated fatty acids, and (G) unsaturated fatty acids. DA-CB indicates DA-CB-treated *Msm* cells and control indicates only DMSO-treated *Msm* cells.

(i.e., Tal, HisF, HisG, and GlnA) were significantly decreased. The proteins involved in the biosynthesis of fatty acids,  $\alpha$ -linolenic acid metabolism, fatty acid metabolism, fatty acid degradation, and pantothenate and CoA biosynthesis were also significantly decreased (Table 3). This decrease in proteins associated with fatty acid metabolism could be in response to the observed accumulation of various fatty acids, which has been associated with cellular toxicity.<sup>53,54</sup>

**Integration of Metabolomics and Proteomics Data Demonstrates that DA-CB-Altered Pathways Are Associated with Nitrogen-Containing Metabolites.** Both the metabolomics and proteomics data sets revealed that pyrimidine biosynthesis was affected by DA-CB treatment (Figures 3A and 6B). The proteins involved in pyrimidine metabolism pathway orotate phosphoribosyltransferase (PyrE), thymidylate kinase (dTMP kinase, MSMEG\_1873), thioredoxin (Trx), and cytosine deaminase (MSMEG\_4687) were significantly decreased in cells treated with DA-CB compared to controls (Table 3). PyrE plays a vital role in

pyrimidine biosynthesis since it synthesizes orotidine 5'-monophosphate, which is a key precursor in the *de novo* pyrimidine biosynthesis pathway.<sup>55</sup> PyrE also catalyzes the conversion of  $\alpha$ -D-5-phosphoribosyl-1-pyrophosphate and orotate into pyrophosphate and orotidine 5'-monophosphate, respectively. The metabolomics data was also consistent with the downregulation of PyrE since pyrimidine metabolites downstream of PyrE were significantly decreased. For example, uridine-diphosphate and UDP-GlcNAC were decreased in DA-CB-treated cells (Table 1). Thus, a disruption in pyrimidine biosynthesis may contribute to the MoA of DA-CB in arresting *Msm* growth. Although the proteomics enrichment results did not identify purine metabolism as the most impacted pathway, the metabolomics data set did. DA-CB depleted methylthioadenosine and deoxyguanosine and increased cyclic AMP and deoxy guanosine-monophosphate. Proteins associated with purine metabolism, such as ATP-synthase subunit (AtbB), pyrophosphatase (RdgB), and phosphoribosylformylglycinamide cyclo-ligase (PurM), were downregulated in DA-CB-

Table 2. Lipids Significantly Altered by DA-CB Treatment

categories	class	subclass	lipid maps (common names)	VIP OPLS <sup>a</sup>	p-value <sup>b</sup>	FDR-corrected p-value <sup>c</sup>	FC <sup>d</sup>	
fatty acyls	fatty acids	branched chain fatty acids	methyl-hexacosanoic acid	1.25	$2.90 \times 10^{-17}$	$2.7748 \times 10^{-16}$	1609.95	
			diabolic acid	1.23	$5.05 \times 10^{-16}$	$3.38179 \times 10^{-15}$	972.47	
	hydroxy fatty acids	hydroxy fatty acids	hydroxyphthioiceric acid (C40)	1.25	$1.33 \times 10^{-13}$	$3.07911 \times 10^{-13}$	3.10	
			mycolipanoic acid (C24)	1.24	$1.45 \times 10^{-11}$	$2.02569 \times 10^{-11}$	8.94	
			mycosanoic acid (C24)	1.25	$6.77 \times 10^{-16}$	$3.7773 \times 10^{-15}$	80.14	
			corynomycolic acid	1.18	$4.01 \times 10^{-8}$	$4.4431 \times 10^{-8}$	0.28	
			hydroxy-tetracosanoic acid	1.17	$4.65 \times 10^{-7}$	$4.86822 \times 10^{-7}$	2.71	
			hydroxy-triacontanoic acid	1.21	$1.14 \times 10^{-9}$	$1.33741 \times 10^{-9}$	0.18	
			lanoceric acid	1.24	$5.81 \times 10^{-14}$	$1.62335 \times 10^{-13}$	6.77	
			eicosyl-hydroxy-oxo-methyl-nonatetracontanoic acid	1.18	$4.08 \times 10^{-6}$	$4.20735 \times 10^{-6}$	0.58	
			tetracosyl-hydroxy-carboxy-octatriacontanoic acid	1.18	$1.28 \times 10^{-13}$	$3.05092 \times 10^{-13}$	0.49	
			alpha-mycolic acid	1.10	$1.39 \times 10^{-9}$	$1.60496 \times 10^{-9}$	0.53	
	saturated fatty acids	saturated fatty acids	keto meromycolic acid	1.05	$3.46 \times 10^{-10}$	$4.37198 \times 10^{-10}$	0.57	
			arachidic acid	1.25	$6.52 \times 10^{-13}$	$1.24799 \times 10^{-12}$	9.38	
			behenic acid	1.25	$5.83 \times 10^{-13}$	$1.14791 \times 10^{-12}$	36.33	
			nonacosenoic acid	1.24	$1.24 \times 10^{-11}$	$1.76927 \times 10^{-11}$	8.77	
	unsaturated fatty acids	unsaturated fatty acids	dotriacontanoic acid	1.24	$9.10 \times 10^{-12}$	$1.32584 \times 10^{-11}$	3.36	
			FA(28:2)	1.24	$1.12 \times 10^{-13}$	$2.76861 \times 10^{-13}$	23.50	
			FA(32:4)	1.23	$1.40 \times 10^{-12}$	$2.40122 \times 10^{-12}$	10.91	
			myristoleyl myristate	1.25	$2.00 \times 10^{-14}$	$6.68573 \times 10^{-14}$	15.07	
myristyl linoleate			1.25	$2.03 \times 10^{-12}$	$3.34994 \times 10^{-12}$	22.49		
nonadecyl palmitoleate			1.25	$1.44 \times 10^{-8}$	$1.63753 \times 10^{-8}$	46.80		
oleyl palmitoleate			1.25	$4.17 \times 10^{-12}$	$6.6483 \times 10^{-12}$	21.26		
pentacosanyl palmitoleate			1.25	$3.25 \times 10^{-16}$	$2.71997 \times 10^{-15}$	748.57		
tetracosanyl palmitoleate			1.24	$6.94 \times 10^{-13}$	$1.29192 \times 10^{-12}$	3.40		
tricosanyl palmitoleate			1.24	$4.52 \times 10^{-14}$	$1.31597 \times 10^{-13}$	3.99		
diacylglycerols	diacylglycerols	DG(14:1,14:1)	1.25	$2.32 \times 10^{-13}$	$4.86543 \times 10^{-13}$	33.42		
		DG(15:0,18:0)	1.24	$5.21 \times 10^{-10}$	$6.46664 \times 10^{-10}$	2.09		
		DG(17:1,22:0)	1.25	$1.15 \times 10^{-14}$	$4.04228 \times 10^{-14}$	3.39		
		DG(19:0,22:0)	1.24	$1.38 \times 10^{-13}$	$3.07911 \times 10^{-13}$	2.28		
		TG(12:0,12:0,18:3)	1.25	$8.19 \times 10^{-12}$	$1.21997 \times 10^{-11}$	21.71		
		TG(12:0,12:0,18:4)	1.25	$3.11 \times 10^{-14}$	$9.67007 \times 10^{-14}$	48.57		
		TG(12:0,12:0,20:4)	1.25	$4.03 \times 10^{-11}$	$5.39532 \times 10^{-11}$	21.09		
		TG(12:0,14:1,18:4)	1.25	$2.97 \times 10^{-11}$	$4.0635 \times 10^{-11}$	10.25		
		TG(18:0,20:4,22:6)	1.22	$1.05 \times 10^{-4}$	0.000106722	43.49		
		TG(18:2,22:3,22:6)	1.25	$7.93 \times 10^{-18}$	$1.06267 \times 10^{-16}$	3.28		
triacylglycerols	triacylglycerols	TG(18:3,20:5,22:0)	1.24	$1.98 \times 10^{-20}$	$1.32374 \times 10^{-18}$	16.52		
		PA(18:1,18:4)	1.24	$3.53 \times 10^{-15}$	$1.57472 \times 10^{-14}$	5.47		
		PC(22:0,24:1)	1.24	$1.14 \times 10^{-19}$	$2.55173 \times 10^{-18}$	4.50		
		PE(18:0,18:4)	1.24	$3.18 \times 10^{-14}$	$9.67007 \times 10^{-14}$	402.91		
		PE(19:0,18:3)	1.23	$8.80 \times 10^{-11}$	$1.15588 \times 10^{-10}$	3.08		
		PE(P-16:0,20:3)	1.23	$6.60 \times 10^{-10}$	$8.03472 \times 10^{-10}$	8.36		
		PI(22:1,21:0)	1.24	$1.49 \times 10^{-10}$	$1.91703 \times 10^{-10}$	21.50		
		glycerophospholipids	Glycerophosphotidic acid glycerophospho-choline glycerophospho-ethanolamine	diacyl-glycerophosphotidic acid				
				diacyl-glycerophospho-choline				
				diacyl-glycerophospho-ethanolamine				
diacyl-glycerophospho-inositol								

Table 2. continued

categories	class	subclass	lipid maps (common names)	VIP OPLS <sup>a</sup>	p-value <sup>b</sup>	FDR-corrected p-value <sup>c</sup>	FC <sup>d</sup>
saccharolipids	glycerophosphoserine	diacylglycerophosphoserine	PS(20:3,0:0)	1.21	$8.33 \times 10^{-15}$	$3.09983 \times 10^{-14}$	0.33
	oxidized glycerophospholipid	oxidized glycerophosphates	PON-PG	1.25	$5.98 \times 10^{-15}$	$2.35554 \times 10^{-14}$	1314.68
acyltrehaloses	acyltrehaloses	NA	AC2SGL(18:0,30:0)	1.21	$8.69 \times 10^{-13}$	$1.53137 \times 10^{-12}$	2.55
		NA	DAT(16:0,24:0)	1.25	$1.18 \times 10^{-17}$	$1.32219 \times 10^{-16}$	3.83
		NA	DAT(16:0,25:0)	1.25	$4.22 \times 10^{-20}$	$1.415 \times 10^{-18}$	5.01

<sup>a</sup>VIP score—variable importance in projection score from the OPLS-DA model. <sup>b</sup>p-value—Student's *t*-test p-value. <sup>c</sup>FDR-corrected p-value using the Benjamini–Hochberg method. <sup>d</sup>FC—fold change calculated using the average of the integrated peak area from DA-CB treatments divided by the average of the integrated peak area from control samples.

treated cells. Notably, AtpB is a key component of the proton channel and an important antimycobacterial drug target.<sup>56,57</sup> DA-CB downregulated AtpB 1.8-fold with a *p*-value < 0.05. Additionally, the PPP was among the most altered pathways identified in the proteomics data set. The PPP provides precursors for the biosynthesis of nucleotides (i.e., purine and pyrimidine metabolism) and amino acids.<sup>58</sup> PPP proteins such as 2-dehydro-3-deoxy-phosphogluconate aldolase (Eda), phospho-gluconolactonase (Pgl), transaldolase (Tal), and glucose-6-phosphate 1-dehydrogenase (Zwf) were downregulated in the presence of DA-CB. The PPP is upstream of nucleotide production, and the overall alteration in pyrimidines and purines (i.e., nucleotide biosynthesis) could be due to the PPP depletion associated with DA-CB.

Our metabolomics data revealed that amino acid metabolism was the top enriched pathway in response to DA-CB treatment (Figure 3A). The metabolites identified in this pathway that included acetyl-arginine and ornithine were all increased with the addition of DA-CB (Figure 3B). Some of the observed amino acid changes were also correlated with a downregulation in proteins related to the biosynthesis of amino acids, which included Tal (which also has a role in PPP), imidazole glycerol phosphate synthase subunit (HisF), ATP phosphoribosyl-transferase (HisG), and glutamine synthase (GlnA) (Table 3). GlnA is an essential *Msm* protein with a role as a global nitrogen metabolism regulator.<sup>59</sup> Nitrogen metabolism plays a central role in all bacteria, and our proteomics data identified the organo-nitrogen metabolic process as the third most altered biological process following treatment with DA-CB (Figure 6C). Proteins associated with ribosome, pyrimidine, purine, and amino acid biosynthesis were all altered due to DA-CB. Although major alterations of ribosomal proteins were not inferred from the metabolomic or lipidomic results, some of the affected ribosomal proteins are known to be cell wall associated in *Msm*.<sup>60</sup> The 30S and 50S ribosomal proteins found in the cell wall (RpsR, RplP, and RpsM) were decreased due to DA-CB treatment.

**Integration of Lipidomics and Proteomics Data Substrates DA-CB-Depleted Fatty Acids and Altered Proteins Involved in Cell Wall Biosynthesis.** Alterations in fatty acid metabolism comprised the most common pathway changes inferred from the proteomics and lipidomics data sets. Evidence of an altered lipid metabolism was also present in the metabolomics data set. The biosynthesis of unsaturated fatty acids and fatty acid metabolism were among the most impacted pathways in the proteomics data set. Fatty acid biosynthesis and degradation were also in the enriched pathways (Table 3). The top six enhanced pathways from the lipidomics data set included five different classes of fatty acids: branched chain fatty acids, hydroxy, unsaturated and saturated fatty acids, and mycolic acids (Figure 5). Fatty acid biosynthesis is more complicated in mycobacteria and corynebacteria compared to other bacterial species owing to the presence of both the FAS type I and type II pathways.<sup>61</sup> In these pathways, fatty acids are synthesized by repeated cycles of transacylation.<sup>62</sup>

CoAs and acyl carrier proteins (ACPs), which are essential for priming and extending the growing acyl chain, are the two most important components in fatty acid biosynthesis.<sup>61,62</sup> Indeed, our metabolomics and proteomics data showed alterations in CoA metabolites and ACPs, which suggests that DA-CB may be targeting FAS components. For example, linoleoyl-CoA was increased (Figure 3F), and pantothenic acid

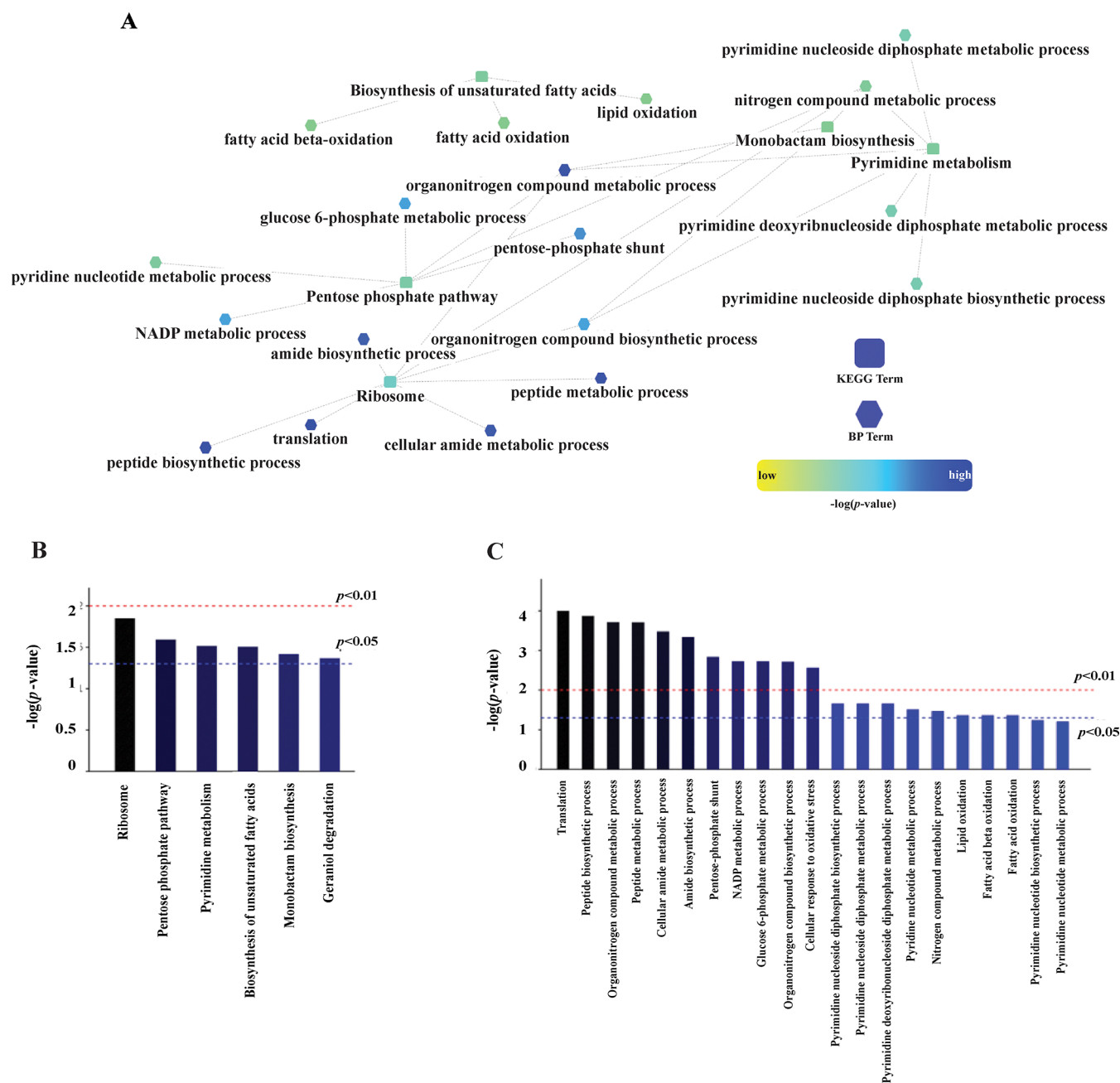


**Figure 6.** (A) Cytoscape (<https://cytoscape.org/>) network generated from the 123 differentially expressed proteins in the proteomics data set and using the *Msm* protein database. Nodes using a square symbol indicate altered pathways from the Kyoto Encyclopedia of Genes and Genomes (KEGG) database, while nodes with a hexagon symbol indicate altered biological processes (BP). Summary of the (B) KEGG and (C) BP terms that were significantly altered according to the network analysis of the proteomics data set.

was decreased (Table S1) in cells treated with DA-CB. Pantothenic acid is the key precursor for the biosynthesis of CoA. CoA is an essential cofactor involved in a myriad of metabolic processes that includes phospholipid biosynthesis and both the degradation and synthesis of fatty acids.<sup>63</sup> The depletion in pantothenic acid could be attributed to alterations in acyl-CoA metabolites (i.e., accumulation of linoleoyl-CoA). ACPs are important for acyl chain elongation and fatty acid biosynthesis and are downregulated in cells treated with DA-CB. Acyl-CoA oxidase (MSMEG\_4474), which is involved in the utilization of fatty acids as carbon sources via beta oxidation, was also downregulated due to DA-CB. In contrast, two acyl-CoA dehydrogenases (FadE5, MSMEG\_4715) were

significantly upregulated in cells treated with DA-CB. Acyl-CoA dehydrogenases introduce unsaturation into the carbon chains during lipid metabolism, which correlates with the observed accumulation of unsaturated fatty acids in cells treated with DA-CB. Recently, Chen et al. (2020) reported that FadE5 from *Mtb* and *Msm* contributed to drug resistance.<sup>64</sup>

Our lipidomics data set showed a significantly lowered production of mycolic acids (Figure SD and Table 2). This is consistent with our prior observation (Figure 1) that a treatment with either DA-CB or ETH was associated with similar global metabolomics changes, which, in turn, suggests a shared general MoA that includes disrupting mycolic acid

Table 3. Top Protein Pathways and Associated Genes Altered by DA-CB Treatment<sup>a</sup>

pathway name	pathway KEGG ID	protein description	UNIPROT gene names	FC <sup>b</sup>	p-value	FDR-corrected p-value <sup>c</sup>
ribosomal proteins	msm03010	30S ribosomal protein	<i>rpsK</i>	0.55	$2.41 \times 10^{-3}$	$2.42 \times 10^{-2}$
		30S ribosomal protein	<i>rpsR2</i>	0.58	$2.47 \times 10^{-2}$	$9.88 \times 10^{-2}$
		50S ribosomal protein	<i>rplP</i>	0.71	$2.46 \times 10^{-2}$	$9.88 \times 10^{-2}$
		30S ribosomal protein	<i>rpsL</i>	0.61	$4.81 \times 10^{-3}$	$3.81 \times 10^{-2}$
		30S ribosomal protein	<i>rpsS</i>	0.72	$2.43 \times 10^{-2}$	$9.88 \times 10^{-2}$
		30S ribosomal protein	<i>rpsM</i>	0.74	$2.91 \times 10^{-2}$	$1.09 \times 10^{-1}$
pentose phosphate pathway	msm00030	2-dehydro-3-deoxy-phosphogluconate aldolase	<i>eda</i>	<b>0.63</b>	$5.81 \times 10^{-3}$	$4.25 \times 10^{-2}$
		6-phosphogluconolactonase	<i>pgl</i>	<b>0.6</b>	$1.05 \times 10^{-2}$	$6.05 \times 10^{-2}$
		<b>transaldolase</b>	<i>tal</i>	<b>0.71</b>	$1.57 \times 10^{-2}$	$8.09 \times 10^{-2}$
		glucose-6-phosphate 1-dehydrogenase	<i>zwf</i>	<b>0.54</b>	$3.67 \times 10^{-3}$	$3.22 \times 10^{-2}$
pyrimidine metabolism	msm00240	<b>orotate phosphoribosyltransferase</b>	<i>pyre</i>	<b>0.57</b>	$3.87 \times 10^{-2}$	$1.28 \times 10^{-1}$
		<b>dTMP kinase</b>	<i>MSMEG_1873</i>	<b>0.65</b>	$1.57 \times 10^{-2}$	$8.09 \times 10^{-2}$
		<b>thioredoxin</b>	<i>trx</i>	<b>0.68</b>	$3.05 \times 10^{-2}$	$1.09 \times 10^{-1}$
biosynthesis of unsaturated fatty acids	MSM01040	short-chain dehydrogenase	<i>MSMEG_0779</i>	<b>0.65</b>	$2.11 \times 10^{-3}$	$2.30 \times 10^{-2}$
		acyl-CoA oxidase	<i>MSMEG_4474</i>	<b>0.7</b>	$9.87 \times 10^{-3}$	$5.95 \times 10^{-2}$
monobactam biosynthesis	msm00261	dihydrodipicolinate reductase	<i>dapB</i>	0.67	$1.61 \times 10^{-2}$	$8.09 \times 10^{-2}$
geraniol degradation	msm00281	sulfate adenylyltransferase subunit	<i>cysD</i>	1.36	$2.70 \times 10^{-2}$	$1.06 \times 10^{-1}$
		enoyl-CoA hydratase	<i>MSMEG_1048</i>	0.67	$2.05 \times 10^{-2}$	$9.19 \times 10^{-2}$
alpha-linolenic acid metabolism	msm00592	acyl-CoA dehydrogenase	<i>MSMEG_4715</i>	1.39	$4.46 \times 10^{-2}$	$1.41 \times 10^{-1}$
		acyl-coA-dehydrogenase	<i>fadE5</i>	1.87	$2.24 \times 10^{-3}$	$2.38 \times 10^{-2}$
		acyl-CoA oxidase	<i>MSMEG_4474</i>	<b>0.7</b>	$9.87 \times 10^{-3}$	$5.95 \times 10^{-2}$
fatty acid metabolism	msm01212	enoyl-CoA hydratase	<i>MSMEG_1048</i>	<b>0.67</b>	$2.05 \times 10^{-2}$	$9.19 \times 10^{-2}$
		short-chain dehydrogenase	<i>MSMEG_0779</i>	<b>0.65</b>	$2.11 \times 10^{-3}$	$2.30 \times 10^{-2}$
		acyl-CoA oxidase	<i>MSMEG_4474</i>	<b>0.7</b>	$9.87 \times 10^{-3}$	$5.95 \times 10^{-2}$
		<b>dihydrodipicolinate reductase</b>	<i>dapB</i>	<b>0.67</b>	$1.61 \times 10^{-2}$	$8.09 \times 10^{-2}$
biosynthesis of amino acids	msm01230	<b>transaldolase</b>	<i>tal</i>	<b>0.71</b>	$1.57 \times 10^{-2}$	$8.09 \times 10^{-2}$
		<b>imidazole glycerol phosphate synthase subunit hisF</b>	<i>hisF</i>	<b>0.54</b>	$1.91 \times 10^{-3}$	$2.15 \times 10^{-2}$
		<b>ATP phosphoribosyltransferase</b>	<i>hisG</i>	<b>0.57</b>	$3.14 \times 10^{-3}$	$1.66 \times 10^{-3}$
		<b>glutamine synthetase</b>	<i>glnA</i>	<b>0.52</b>	$9.43 \times 10^{-5}$	
		<b>holo-[acyl-carrier-protein] synthase</b>	<i>acpS</i>	<b>0.69</b>	$3.06 \times 10^{-2}$	$1.09 \times 10^{-1}$
pantothenate and CoA biosynthesis	msm00770	holo-[acyl-carrier-protein] synthase	<i>acpS</i>	<b>0.69</b>	$3.06 \times 10^{-2}$	$1.09 \times 10^{-1}$
fatty acid biosynthesis	msm00061	short-chain dehydrogenase	<i>MSMEG_0779</i>	<b>0.65</b>	$2.11 \times 10^{-3}$	$2.30 \times 10^{-2}$
fatty acid degradation	msm00071	enoyl-CoA hydratase	<i>MSMEG_1048</i>	0.67	$2.05 \times 10^{-2}$	$9.19 \times 10^{-2}$
		acyl-CoA oxidase	<i>MSMEG_4474</i>	0.7	$9.87 \times 10^{-3}$	$5.95 \times 10^{-2}$
amino sugar and nucleotide sugar metabolism	msm00520	polyphosphate glucokinase	<i>MSMEG_2760</i>	0.34	$1.30 \times 10^{-5}$	$3.25 \times 10^{-4}$

<sup>a</sup>Bolded text identifies pathways that were also identified with the metabolomics data set (Table 1). <sup>b</sup>FC—fold change calculated using the average of the integrated peak area from DA-CB treatments divided by the average of the integrated peak area from control samples. <sup>c</sup>FDR-corrected p-value using the Benjamini–Hochberg method.

biosynthesis. The depletion in mycolic acid synthesis also implicates FAS-I and FAS-II. Importantly, the FAS-II pathway is the committed step to mycolic acid biosynthesis. In total, our multi-omics data provides strong evidence that DA-CB impacts mycolic acid and cell wall biosynthesis through the inhibition of specific enzyme(s) within the FAS pathways. Nataraj et al. (2015) states that the vast majority of the genes involved in mycolic acid biosynthesis are essential for viability and virulence and therefore important targets for drug development.<sup>65–68</sup> Indeed, changes in the structure or composition of mycolic acids have been associated with a modification in cell wall permeability and the attenuation of pathogenic mycobacterial strains.<sup>60</sup> Type I polyketide synthase (*pks13*) and fatty acyl-AMP ligase (*fadD32*) are key proteins in the synthesis of mycolic acids and were identified as essential proteins for the viability of *Msm* and *Mtb*. The biosynthesis of mycolic acids is catalyzed by proteins encoded by the *fadD32*-

*pks13-accD4* cluster.<sup>69,70</sup> The observation that corynomycolic acid and keto-meromycolic acid were both decreased suggests that *Pks13* may be important to the MoA of DA-CB.<sup>71,72</sup> The accumulation of lipid intermediates and the downregulation of the corresponding enzymes as described above in detail further implicates the involvement of the *Pks13* complex with the MoA of DA-CB.

Last, our lipidomics identified wax monoesters as the most altered lipid pathway (Figure 5A). Wax monoesters are known to be synthesized when mycobacteria are exposed to stress (Figure 5B).<sup>73</sup> Thus, our observed increase in wax monoesters implies a stress response in *Msm* cells that is induced by a DA-CB treatment and facilitated by the accumulation of FAS-I and FAS-II metabolites that provide substrates for the stress response. In addition, our proteomics data showed that the two superoxide dismutase enzymes (*SodA*, *MSMEG\_6636*) were significantly downregulated in cells treated with DA-CB. The

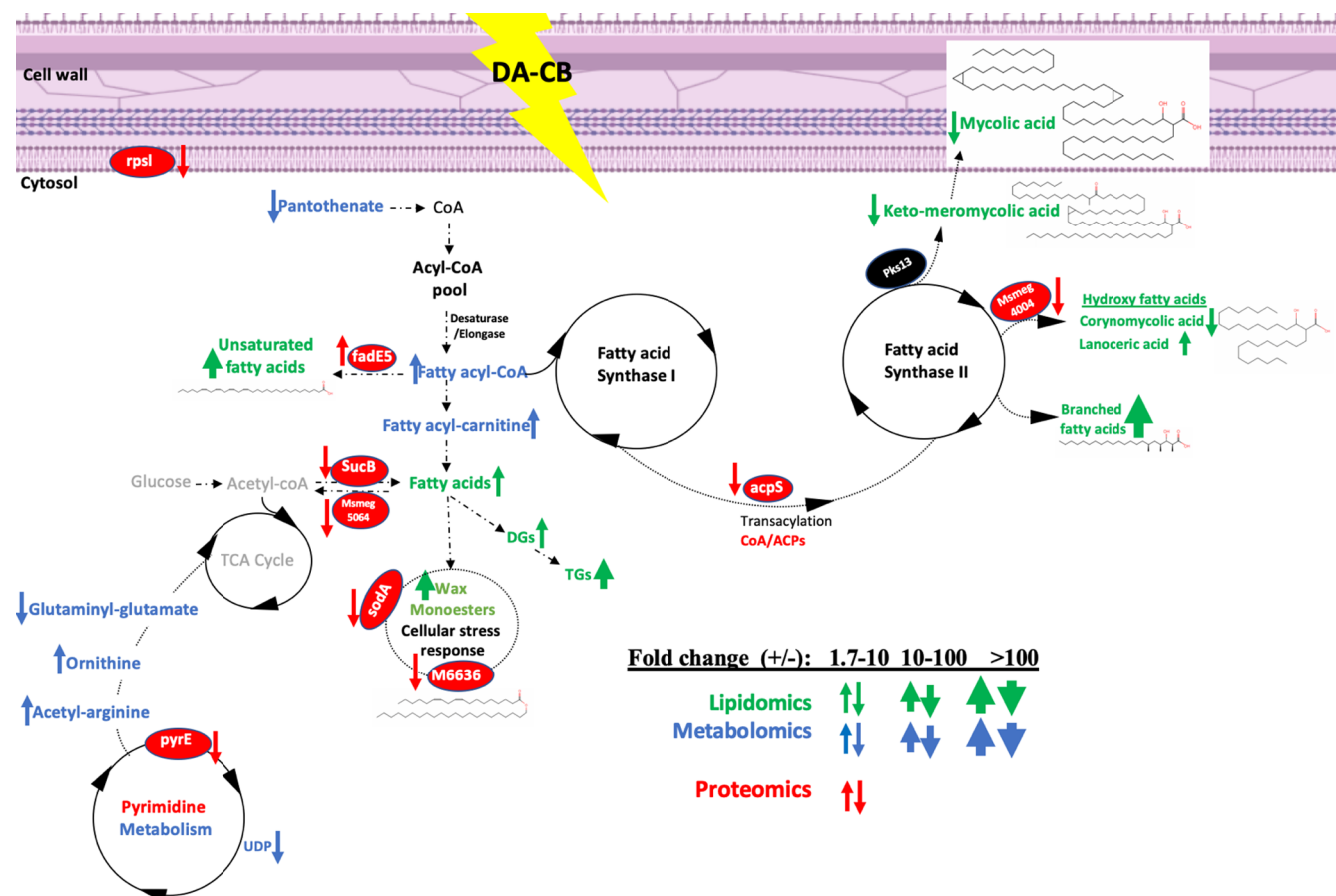


**Figure 7.** Schematic of an integrated network of the multi-omics data sets summarizing the consensus changes in the *Msm* lipidome (green), metabolome (blue), and proteome (red) resulting from DA-CB treatment. An up arrow indicates an increase in cells treated with DA-CB and a down arrow indicates a decrease. The relative thickness of the arrow indicates the range of the fold change for the lipid, metabolite, or protein (inset). A molecule colored black was not detected or altered by DA-CB but was included to highlight important nodes or to connect to other observed nodes.

superoxide dismutases protect the cells against oxidative stress by scavenging superoxide, which contributes to bacterial pathogenicity.<sup>74</sup> Overall, these results suggest that DA-CB induces oxidative stress within mycobacteria, perhaps by downregulating superoxide dismutases that protect cells against oxidative stress.<sup>75</sup>

**Multi-omics Results Show that DA-CB Effects Fatty Acid Biosynthesis and Pyrimidine Biosynthesis.** The pathways common to the proteomics, metabolomics, and lipidomics data sets were combined into a single consensus integrated network (Figure 7). This integrated metabolic pathway provides a clear overview of the system-wide impact of DA-CB treatment on *Msm* and identifies FAS metabolism as the focal point of DA-CB activity. The alteration in pantothenate-CoA biosynthesis and pyrimidine metabolism and the downregulation of ACP synthase (AcpS) further support FAS metabolism as the target of DA-CB inhibition. Pantothenate-CoA biosynthesis and pyrimidine metabolism influence the fatty acyl-CoA pool, which supplies FAS-I, FAS-II, and mycolic acid biosynthesis. AcpS is also an important component of the FAS-I and FAS-II systems. Four (i.e., RpsI, SodA, SucB, and PyrE) other proteins colored red in Figure 7 have been previously identified as being encoded by essential *Msm* genes (Table S4).<sup>76,77</sup>

To provide further support for our consensus integrated network (Figure 7), a Spearman's rank correlation coefficient

was calculated between each of the 26 metabolites, 48 lipids, and 123 proteins that were significantly altered by DA-CB. A hierarchical clustered heatmap that summarizes the entire set of pairwise correlation coefficients are shown in Figure S5. The heatmap shows a strong positive or negative correlation between all the significantly altered metabolites, lipids, and proteins. A network map based on the Spearman's rank correlation coefficients for the 61 metabolites, lipids, and proteins depicted in Figure 7 is shown in Figure S6. The network identified 51 tightly interconnected molecules demonstrating a unified cellular response to the DA-CB treatment and the accuracy of the consensus integrated network. For example, alpha-mycolic acid is positively correlated with all other mycolic acids and negatively correlated with triacylglycerols [i.e., TG(12:0,12:0,20:4)]. Corynomycolic acid is positively correlated with hydroxy-triacontanoic acid (i.e., hydroxy fatty acids) and negatively correlated with PE(18:0,18:4) (i.e., diacyl-glycerophosphoethanolamine). UDP-GlcNAc and deoxythymidine diphosphate-1-rhamnose (i.e., pyrimidine nucleotides) are both negatively correlated with hydroxy-tetracosanoic acid (i.e., hydroxy fatty acid lipids) and myristyl myristate (i.e., a wax monoester).

Overall, our multi-omics data provides complementary lines of evidence that strongly implicates a FAS enzyme as the main inhibitory target of DA-CB in mycolic acid biosynthesis. Specifically, the terminal FAS-II Claisen condensation

catalyzed by Pks13 and the associated FadD32 protein complex are potential candidates for the lethal target of DA-CB. In this regard, DA-CB may function through a direct enzyme inhibition or by the modification of the structure of a lipid precursor. A further investigation into the roles that acyl-CoA oxidase, FadE5, ACP, and cell wall ribosomal proteins (RplP and RpsM) may contribute to the MoA of DA-CB would enhance our understanding of anti-tubercular drugs that target cell wall biosynthesis. AcpS is not an essential gene; however, its downregulation affects transacylation and the further synthesis of FAS-II metabolites such as hydroxy and branched chain fatty acids that are important to mycolic acid biosynthesis (Table S4).<sup>76</sup>

## CONCLUSIONS

In summary, we report the elucidation of a probable MoA for DA-CB, an antimycobacterial fatty acid analogue.<sup>15,16</sup> A multi-omics approach that combined lipidomics, metabolomics, and proteomics provided numerous, reinforcing, and complementary results. Our integrated metabolomics, lipidomics, and proteomics analysis identified alterations in the FAS-II system, specifically in the terminal steps of mycolic acid biosynthesis. We also observed contributing alterations in pyrimidine and amino acids synthesis, and our integrated lipidomics and proteomics analysis identified alterations in FAS, specifically in mycolic acid biosynthesis. A consensus network (Figure 7) integrated these multi-omics data sets and provided a system-wide view of the cellular impact of DA-CB on the metabolome of *Msm*. The similarity in the global metabolic perturbations induced by both DA-CB and ETH, a known inhibitor of mycolic acid biosynthesis, provides further support for our proposed MoA.<sup>27,78</sup> However, the inhibited enzyme is different from InhA, the target of ETH, since we observed an overproduction (instead of a decrease) in hydroxy fatty acids and branched chain fatty acids. This outcome also confirms our original hypothesis that a fatty acid analogue such as DA-CB could interrupt fatty acid synthesis or processing, which would lead to mycobacterial cell death. Our proposed MoA is expected to guide future investigations into the confirmation of the precise lethal target(s) of DA-CB. Finding the lethal target of a novel drug often requires intensive dedicated research. For example, the discovery that D-Ala-D-Ala ligase was the lethal target of DCS came 50 years after the introduction of the drug.<sup>35</sup> However, recent developments in omics analysis may hasten this pace.

DA-CB also provides a unique opportunity to leverage click chemistry and to identify target proteins. DA-CB was selected from among a group of related analogues for further study because of its efficacy and because we and others have shown DA-CB and related cyclobutenes undergo rapid and “biorthogonal” click modification in the form of inverse electron demand Diels–Alder cycloadditions with biotinylated 1,2,4,5-tetrazines.<sup>79</sup> The ability to specifically address DA-CB, or any derived biosynthetic intermediates, will provide a unique opportunity to study the localization and/or conjugation of the fatty acid analogues within mycobacteria by using a pull-down assay or chemical cross-linking.<sup>17</sup> As described in the literature, labeling the fatty acid analogue enables tracking of the altered pathways.<sup>30</sup> The same approach may be used for DA-CB, in order to track its incorporation into the fatty acid biosynthetic FAS-I and FAS-II machinery via a fatty acid CoA analogue. Furthermore, the future experiment

of labeling DA-CB will enable us to determine its uptake to understand lipid synthesis changes in *Msm* and *Mtb*.

## ASSOCIATED CONTENT

### Supporting Information

The Supporting Information is available free of charge at <https://pubs.acs.org/doi/10.1021/jacs.2c08238>.

Experimental details, summary of the analysis of NMR metabolomics data, volcano plot summarizing proteomics data, interaction network of proteins altered by DA-CB treatment, heatmap and network map based on Spearman's rank correlation coefficients, summary of quality and validation metrics for the PCA and OPLS-DA models, *Msm* protein expression significantly altered ( $p$ -value < 0.01) by DA-CB treatment, and essentiality of genes expressing proteins that were significantly altered by the DA-CB treatment (PDF)

List of Spearman's rank correlation coefficients calculated between the 197 DA-CB altered molecules (XLSX)

## AUTHOR INFORMATION

### Corresponding Author

**Robert Powers** – Department of Chemistry and Nebraska Center for Integrated Biomolecular Communication, University of Nebraska-Lincoln, Lincoln, Nebraska 68588-0304, United States; Redox Biology Center, University of Nebraska-Lincoln, Lincoln, Nebraska 68588-0664, United States; [orcid.org/0000-0001-9948-6837](https://orcid.org/0000-0001-9948-6837); Phone: (402) 472-3039; Email: [rpowers3@unl.edu](mailto:rpowers3@unl.edu); Fax: (402) 472-9402

### Authors

**Isin T. Sakallioglu** – Department of Chemistry, University of Nebraska-Lincoln, Lincoln, Nebraska 68588-0304, United States; [orcid.org/0000-0001-9059-2705](https://orcid.org/0000-0001-9059-2705)

**Amith S. Maroli** – Department of Chemistry and Nebraska Center for Integrated Biomolecular Communication, University of Nebraska-Lincoln, Lincoln, Nebraska 68588-0304, United States; Present Address: NYS Center for Clean Water Technology, Stony Brook University, Stony Brook, New York 11794, United States; [orcid.org/0000-0002-0647-0316](https://orcid.org/0000-0002-0647-0316)

**Aline De Lima Leite** – Department of Chemistry and Nebraska Center for Integrated Biomolecular Communication, University of Nebraska-Lincoln, Lincoln, Nebraska 68588-0304, United States; [orcid.org/0000-0002-2112-1309](https://orcid.org/0000-0002-2112-1309)

**Darrell D. Marshall** – Department of Chemistry, University of Nebraska-Lincoln, Lincoln, Nebraska 68588-0304, United States; Total Analysis LLC, Detroit, Michigan 48204-3268, United States

**Boone W. Evans** – Department of Chemistry, University of Nebraska-Lincoln, Lincoln, Nebraska 68588-0304, United States; Present Address: Rieke Metals LLC, Lincoln, Nebraska 68521, United States

**Denise K. Zinniel** – School of Veterinary Medicine and Biomedical Sciences, University of Nebraska-Lincoln, Lincoln, Nebraska 68583-0905, United States

**Patrick H. Dussault** – Department of Chemistry, University of Nebraska-Lincoln, Lincoln, Nebraska 68588-0304, United States; [orcid.org/0000-0002-9834-1350](https://orcid.org/0000-0002-9834-1350)

Raúl G. Barletta – School of Veterinary Medicine and Biomedical Sciences, University of Nebraska-Lincoln, Lincoln, Nebraska 68583-0905, United States; Redox Biology Center, University of Nebraska-Lincoln, Lincoln, Nebraska 68588-0664, United States; [orcid.org/0000-0002-2278-2563](https://orcid.org/0000-0002-2278-2563)

Complete contact information is available at:  
<https://pubs.acs.org/10.1021/jacs.2c08238>

## Notes

The authors declare no competing financial interest.

## ACKNOWLEDGMENTS

This work was supported in part by funding from the Redox Biology Center (P30 GM103335, NIGMS, R.P., and R.G.B.) and the Nebraska Center for Integrated Biomolecular Communication (P20 GM113126, NIGMS, A.S.M., A.D.L.L., and R.P.). The research was performed in facilities renovated with support from the National Institutes of Health (RR015468-01, I.T.S., A.S.M., A.D.L.L., D.D.M., B.W.E., P.H.D., and R.P.). This project was also supported by the Nebraska Agricultural Experiment Station with funding from the USDA National Institute of Food and Agriculture (NEB-39-178 and NEB-39-179, R.G.B.).

## REFERENCES

- (1) Smith, I. Mycobacterium tuberculosis pathogenesis and molecular determinants of virulence. *Clin. Microbiol. Rev.* **2003**, *16*, 463–496.
- (2) Geneva: World Health Organization. *Global Tuberculosis Report 2021*; WHO Press, 2021.
- (3) Mirzayev, F.; Viney, K.; Linh, N. N.; Gonzalez-Angulo, L.; Gegia, M.; Jaramillo, E.; Zignol, M.; Kasaeva, T. World Health Organization recommendations on the treatment of drug-resistant tuberculosis, 2020 update. *Eur. Respir. J.* **2021**, *57*, 2003300.
- (4) Caminero, J. A.; Matteelli, A.; Lange, C. Treatment of TB. *Eur. Respir. Monogr.* **2012**, *58*, 154–166.
- (5) Chakaya, J.; Khan, M.; Ntoumi, F.; Akillu, E.; Fatima, R.; Mwaba, P.; Kapata, N.; Mfinanga, S.; Hasnain, S. E.; Katoto, P. D. M. C.; Bulabula, A. N. H.; Sam-Agudu, N. A.; Nachega, J. B.; Tiberi, S.; McHugh, T. D.; Abubakar, I.; Zumla, A. Global Tuberculosis Report 2020 - Reflections on the Global TB burden, treatment and prevention efforts. *Int. J. Infect. Dis.* **2021**, *113*, S7.
- (6) Engelbrecht, M. C.; Kigozi, N. G.; Chikobvu, P.; Botha, S.; van Rensburg, H. C. J. Unsuccessful TB treatment outcomes with a focus on HIV co-infected cases: a cross-sectional retrospective record review in a high-burdened province of South Africa. *BMC Health Serv. Res.* **2017**, *17*, 470.
- (7) Leibert, E.; Rom, W. N. New drugs and regimens for treatment of TB. *Expert Rev. Anti Infect. Ther.* **2010**, *8*, 801–813.
- (8) Ormerod, L. P. Multidrug-resistant tuberculosis (MDR-TB): epidemiology, prevention and treatment. *Br. Med. Bull.* **2005**, *73–74*, 17–24.
- (9) Caminero, J. A.; Sotgiu, G.; Zumla, A.; Migliori, G. B. Best drug treatment for multidrug-resistant and extensively drug-resistant tuberculosis. *Lancet Infect. Dis.* **2010**, *10*, 621–629.
- (10) Almeida Da Silva, P. E.; Palomino, J. C. Molecular basis and mechanisms of drug resistance in Mycobacterium tuberculosis: classical and new drugs. *J. Antimicrob. Chemother.* **2011**, *66*, 1417–1430.
- (11) Gandhi, N. R.; Nunn, P.; Dheda, K.; Schaaf, H. S.; Zignol, M.; van Soolingen, D.; Jensen, P.; Bayona, J. Multidrug-resistant and extensively drug-resistant tuberculosis: a threat to global control of tuberculosis. *Lancet* **2010**, *375*, 1830–1843.
- (12) Shah, N. S.; Wright, A.; Bai, G.-H.; Barrera, L.; Boulahbal, F.; Martín-Casabona, N.; Drobniewski, F.; Gilpin, C.; Havelková, M.; Lepe, R.; Lumb, R.; Metchock, B.; Portaels, F.; Rodrigues, M. F.;

Rüsch-Gerdes, S.; Van Deun, A.; Vincent, V.; Laserson, K.; Wells, C.; Cegielski, J. P. Worldwide emergence of extensively drug-resistant tuberculosis. *Emerg. Infect. Dis.* **2007**, *13*, 380–387.

(13) Zhang, Y.; Yew, W. W. Mechanisms of drug resistance in Mycobacterium tuberculosis. *Int. J. Tuberc. Lung Dis.* **2009**, *13*, 1320–30.

(14) Koul, A.; Arnoult, E.; Lounis, N.; Guillemont, J.; Andries, K. The challenge of new drug discovery for tuberculosis. *Nature (London, U.K.)* **2011**, *469*, 483–490.

(15) Sittiwong, W.; Zinniel, D. K.; Fenton, R. J.; Marshall, D. D.; Story, C. B.; Kim, B.; Lee, J. Y.; Powers, R.; Barletta, R. G.; Dussault, P. H. Development of cyclobutene- and cyclobutane-functionalized fatty acids with inhibitory activity against Mycobacterium tuberculosis. *ChemMedChem* **2014**, *9*, 1838–49.

(16) Zinniel, D. K.; Sittiwong, W.; Marshall, D. D.; Rathnaiah, G.; Sakallioglu, I. T.; Powers, R.; Dussault, P. H.; Barletta, R. G. Novel Amphiphilic Cyclobutene and Cyclobutane cis-C18 Fatty Acid Derivatives Inhibit Mycobacterium avium subsp. paratuberculosis Growth. *Vet. Sci.* **2019**, *6*, 46.

(17) Knall, A. C.; Slugovc, C. Inverse electron demand Diels-Alder (iEDDA)-initiated conjugation: a (high) potential click chemistry scheme. *Chem. Soc. Rev.* **2013**, *42*, 5131–5142.

(18) Kim, E.; Koo, H. Biomedical applications of copper-free click chemistry: in vitro, in vivo, and ex vivo. *Chem. Sci.* **2019**, *10*, 7835–7851.

(19) Deb, T.; Tu, J.; Franzini, R. M. Mechanisms and Substituent Effects of Metal-Free Bioorthogonal Reactions. *Chem. Rev.* **2021**, *121*, 6850–6914.

(20) Fang, M. Y.; Huang, K. H.; Tu, W. J.; Chen, Y. T.; Pan, P. Y.; Hsiao, W. C.; Ke, Y. Y.; Tsou, L. K.; Zhang, M. M. Chemoproteomic profiling reveals cellular targets of nitro-fatty acids. *Redox Biol.* **2021**, *46*, 102126.

(21) Bhat, Z. S.; Rather, M. A.; Maqbool, M.; Lah, H. U.; Yousuf, S. K.; Ahmad, Z. Cell wall: A versatile fountain of drug targets in Mycobacterium tuberculosis. *Biomed. Pharmacother.* **2017**, *95*, 1520–1534.

(22) Li, M.; Patel, H. V.; Cognetta, A. B., 3rd; Smith, T. C., 2nd; Mallick, I.; Cavalier, J. F.; Previti, M. L.; Canaan, S.; Aldridge, B. B.; Cravatt, B. F.; Seeliger, J. C. Identification of cell wall synthesis inhibitors active against Mycobacterium tuberculosis by competitive activity-based protein profiling. *Cell Chem. Biol.* **2022**, *29*, 883–896.

(23) Fu, J.; Fu, H.; Dieu, M.; Halloum, I.; Kremer, L.; Xia, Y.; Pan, W.; Vincent, S. P. Identification of inhibitors targeting Mycobacterium tuberculosis cell wall biosynthesis via dynamic combinatorial chemistry. *Chem. Commun.* **2017**, *53*, 10632–10635.

(24) Keating, T.; Lethbridge, S.; Allnut, J. C.; Hendon-Dunn, C. L.; Thomas, S. R.; Alderwick, L. J.; Taylor, S. C.; Bacon, J. Mycobacterium tuberculosis modifies cell wall carbohydrates during biofilm growth with a concomitant reduction in complement activation. *Cell Surf.* **2021**, *7*, 100065.

(25) Banerjee, D.; Bhattacharyya, R. Isoniazid and thioacetazone may exhibit anti-tubercular activity by binding directly with the active site of mycolic acid cyclopropane synthase: Hypothesis based on computational analysis. *Bioinformation* **2012**, *8*, 787–789.

(26) Quémard, A.; Lacave, C.; Lanéelle, G. Isoniazid inhibition of mycolic acid synthesis by cell extracts of sensitive and resistant strains of Mycobacterium aurum. *Antimicrob. Agents Chemother.* **1991**, *35*, 1035–1039.

(27) Quémard, A.; Lanéelle, G.; Lacave, C. Mycolic acid synthesis: a target for ethionamide in mycobacteria? *Antimicrob. Agents Chemother.* **1992**, *36*, 1316–1321.

(28) Winder, F. G.; Collins, P. B.; Whelan, D. Effects of ethionamide and isoxyl on mycolic acid synthesis in Mycobacterium tuberculosis BCG. *J. Gen. Microbiol.* **1971**, *66*, 379–380.

(29) Marrakchi, H.; Lanéelle, M. A.; Daffé, M. Mycolic acids: structures, biosynthesis, and beyond. *Chem. Biol.* **2014**, *21*, 67–85.

(30) Morbidoni, H. R.; Vilchère, C.; Kremer, L.; Bittman, R.; Sacchetti, J. C.; Jacobs, W. R., Jr. Dual inhibition of mycobacterial

fatty acid biosynthesis and degradation by 2-alkynoic acids. *Chem. Biol.* **2006**, *13*, 297–307.

(31) Tran, J. C.; Zamdborg, L.; Ahlf, D. R.; Lee, J. E.; Catherman, A. D.; Durbin, K. R.; Tipton, J. D.; Vellaichamy, A.; Kellie, J. F.; Li, M.; Wu, C.; Sweet, S. M.; Early, B. P.; Siuti, N.; LeDuc, R. D.; Compton, P. D.; Thomas, P. M.; Kelleher, N. L. Mapping intact protein isoforms in discovery mode using top-down proteomics. *Nature* **2011**, *480*, 254–258.

(32) Powers, R. NMR metabolomics and drug discovery. *Magn. Reson. Chem.* **2009**, *47*, S2.

(33) Wishart, D. S. Emerging applications of metabolomics in drug discovery and precision medicine. *Nat. Rev. Drug Discovery* **2016**, *15*, 473–484.

(34) Sakallioğlu, I. T.; Barletta, R. G.; Dussault, P. H.; Powers, R. Deciphering the mechanism of action of antitubercular compounds with metabolomics. *Comput. Struct. Biotechnol. J.* **2021**, *19*, 4284–4299.

(35) Halouska, S.; Chacon, O.; Fenton, R. J.; Zinniel, D. K.; Barletta, R. G.; Powers, R. Use of NMR metabolomics to analyze the targets of D-cycloserine in mycobacteria: role of D-alanine racemase. *J. Proteome Res.* **2007**, *6*, 4608–4614.

(36) Halouska, S.; Fenton, R. J.; Barletta, R. G.; Powers, R. Predicting the in vivo mechanism of action for drug leads using NMR metabolomics. *ACS Chem. Biol.* **2012**, *7*, 166–171.

(37) Baptista, R.; Fazakerley, D. M.; Beckmann, M.; Baillie, L.; Mur, L. A. J. Untargeted metabolomics reveals a new mode of action of pretomanid (PA-824). *Sci. Rep.* **2018**, *8*, 5084.

(38) Dehairs, J.; Derua, R.; Rueda-Rincon, N.; Swinnen, J. V. Lipidomics in drug development. *Drug Discov. Today Technol.* **2015**, *13*, 33–38.

(39) Ahluwalia, K.; Ebricht, B.; Chow, K.; Dave, P.; Mead, A.; Poble, R.; Louie, S. G.; Asante, I. Lipidomics in Understanding Pathophysiology and Pharmacologic Effects in Inflammatory Diseases: Considerations for Drug Development. *Metabolites* **2022**, *12*, 333.

(40) Biagiotti, M.; Dominguez, S.; Yamout, N.; Zufferey, R. Lipidomics and anti-trypanosomatid chemotherapy. *Clin. Transl. Med.* **2017**, *6*, 27.

(41) Ebrahim, A.; Brunk, E.; Tan, J.; O'Brien, E. J.; Kim, D.; Szubin, R.; Lerman, J. A.; Lechner, A.; Sastry, A.; Bordbar, A.; Feist, A. M.; Palsson, B. O. Multi-omic data integration enables discovery of hidden biological regularities. *Nat. Commun.* **2016**, *7*, 13091.

(42) Selevsek, N.; Caiment, F.; Nudischer, R.; Gmuender, H.; Agarkova, I.; Atkinson, F. L.; Bachmann, I.; Baier, V.; Barel, G.; Bauer, C.; Boerno, S.; Bosc, N.; Clayton, O.; Cordes, H.; Deebe, S.; Gotta, S.; Guye, P.; Hersey, A.; Hunter, F. M. I.; Kunz, L.; Lewalle, A.; Lienhard, M.; Merken, J.; Minguet, J.; Oliveira, B.; Pluess, C.; Sarkans, U.; Schrooders, Y.; Schuchhardt, J.; Smit, I.; Thiel, C.; Timmermann, B.; Verheijen, M.; Wittenberger, T.; Wolski, W.; Zerck, A.; Heymans, S.; Kuepfer, L.; Roth, A.; Schlappbach, R.; Niederer, S.; Herwig, R.; Kleinjans, J. Network integration and modelling of dynamic drug responses at multi-omics levels. *Commun. Biol.* **2020**, *3*, 573.

(43) Wang, X.; Zhang, A.; Yan, G.; Sun, W.; Han, Y.; Sun, H. Metabolomics and proteomics annotate therapeutic properties of geniposide: targeting and regulating multiple perturbed pathways. *PLoS One* **2013**, *8*, No. e71403.

(44) Zhang, H. W.; Lv, C.; Zhang, L. J.; Guo, X.; Shen, Y. W.; Nagle, D. G.; Zhou, Y. D.; Liu, S. H.; Zhang, W. D.; Luan, X. Application of omics- and multi-omics-based techniques for natural product target discovery. *Biomed. Pharmacother.* **2021**, *141*, 111833.

(45) Chauhan, A.; Kumar, M.; Kumar, A.; Kanchan, K. Comprehensive review on mechanism of action, resistance and evolution of antimycobacterial drugs. *Life Sci.* **2021**, *274*, 119301.

(46) Flipo, M.; Frita, R.; Bourotte, M.; Martínez-Martínez, M. S.; Boesche, M.; Boyle, G. W.; Derimanov, G.; Drewes, G.; Gamallo, P.; Ghidelli-Disse, S.; Gresham, S.; Jiménez, E.; de Mercado, J.; Pérez-Herrán, E.; Porras-De Francisco, E.; Rullas, J.; Casado, P.; Leroux, F.; Piveteau, C.; Kiass, M.; Mathys, V.; Soetaert, K.; Megalizzi, V.; Tanina, A.; Wintjens, R.; Antoine, R.; Brodin, P.; Delorme, V.;

Moune, M.; Djaout, K.; Slupek, S.; Kemmer, C.; Gitzinger, M.; Ballell, L.; Mendoza-Losana, A.; Lociuero, S.; Deprez, B.; Barros-Aguirre, D.; Remuiñán, M. J.; Willand, N.; Baulard, A. R. The small-molecule SMARt751 reverses Mycobacterium tuberculosis resistance to ethionamide in acute and chronic mouse models of tuberculosis. *Sci. Transl. Med.* **2022**, *14*, No. eaaz6280.

(47) Vale, N.; Gomes, P.; Santos, H. A. Metabolism of the antituberculosis drug ethionamide. *Curr. Drug Metab.* **2013**, *14*, 151–158.

(48) Song, Y.; Wang, G.; Li, Q.; Liu, R.; Ma, L.; Li, Q.; Gao, M. The Value of the inhA Mutation Detection in Predicting Ethionamide Resistance Using Melting Curve Technology. *Infect. Drug Resist.* **2021**, *14*, 329–334.

(49) Sakallioğlu, I. T.; Maroli, A. S.; Leite, A. L.; Powers, R. A reversed phase ultra-high-performance liquid chromatography-data independent mass spectrometry method for the rapid identification of mycobacterial lipids. *J. Chromatogr. A* **2022**, *1662*, 462739.

(50) Lloyd, G. R.; Jankevics, A.; Weber, R. J. M. Struct: an R/bioconductor-based framework for standardised metabolomics data analysis and beyond. *Bioinformatics* **2020**, *36*, 5551–5552.

(51) Pang, Z.; Chong, J.; Zhou, G.; de Lima Morais, D. A.; Chang, L.; Barrette, M.; Gauthier, C.; Jacques, P. E.; Li, S.; Xia, J. MetaboAnalyst 5.0: narrowing the gap between raw spectra and functional insights. *Nucleic Acids Res.* **2021**, *49*, W388–W396.

(52) Bhinderwala, F.; Wase, N.; DiRusso, C.; Powers, R. Combining Mass Spectrometry and NMR Improves Metabolite Detection and Annotation. *J. Proteome Res.* **2018**, *17*, 4017–4022.

(53) Dubos, R. J. The Effect of Lipids and Serum Albumin on Bacterial Growth. *J. Exp. Med.* **1947**, *85*, 9–22.

(54) Lee, W.; VanderVen, B. C.; Fahey, R. J.; Russell, D. G. Intracellular Mycobacterium tuberculosis exploits host-derived fatty acids to limit metabolic stress. *J. Biol. Chem.* **2013**, *288*, 6788–6800.

(55) Donini, S.; Ferraris, D. M.; Miggiano, R.; Massarotti, A.; Rizzi, M. Structural investigations on orotate phosphoribosyltransferase from Mycobacterium tuberculosis, a key enzyme of the de novo pyrimidine biosynthesis. *Sci. Rep.* **2017**, *7*, 1180.

(56) Lu, P.; Lill, H.; Bald, D. ATP synthase in mycobacteria: special features and implications for a function as drug target. *Biochim. Biophys. Acta* **2014**, *1837*, 1208–1218.

(57) McNeil, M. B.; Ryburn, H. W. K.; Harold, L. K.; Tirados, J. F.; Cook, G. M. Transcriptional Inhibition of the F1F0-Type ATP Synthase Has Bactericidal Consequences on the Viability of Mycobacteria. *Antimicrob. Agents Chemother.* **2020**, *64*, No. e00492.

(58) Stincone, A.; Prigione, A.; Cramer, T.; Wamelink, M. M.; Campbell, K.; Cheung, E.; Olin-Sandoval, V.; Grüning, N. M.; Krüger, A.; Tauqeer Alam, M.; Keller, M. A.; Breitenbach, M.; Brindle, K. M.; Rabinowitz, J. D.; Ralser, M. The return of metabolism: biochemistry and physiology of the pentose phosphate pathway. *Biol. Rev. Cambridge Philos. Soc.* **2015**, *90*, 927–963.

(59) Rakovitsky, N.; Bar Oz, M.; Goldberg, K.; Gibbons, S.; Zimhony, O.; Barkan, D. The Unexpected Essentiality of glnA2 in Mycobacterium smegmatis Is Salvaged by Overexpression of the Global Nitrogen Regulator glnR, but Not by L-, D- or Iso-Glutamine. *Front. Microbiol.* **2018**, *9*, 2143.

(60) He, Z.; De Buck, J. Cell wall proteome analysis of Mycobacterium smegmatis strain MC2 155. *BMC Microbiol.* **2010**, *10*, 121.

(61) Elad, N.; Baron, S.; Peleg, Y.; Albeck, S.; Grunwald, J.; Raviv, G.; Shakked, Z.; Zimhony, O.; Diskin, R. Structure of Type-I Mycobacterium tuberculosis fatty acid synthase at 3.3 Å resolution. *Nat. Commun.* **2018**, *9*, 3886.

(62) Gokulan, K.; Aggarwal, A.; Shipman, L.; Besra, G. S.; Sacchettini, J. C. Mycobacterium tuberculosis acyl carrier protein synthase adopts two different pH-dependent structural conformations. *Acta Crystallogr., Sect. D: Biol. Crystallogr.* **2011**, *67*, 657–669.

(63) Leonardi, R.; Jackowski, S. Biosynthesis of Pantothenic Acid and Coenzyme A. *EcoSal Plus* **2007**, *2*, DOI: 10.1128/ecosal-plus.3.6.3.4.

(64) Chen, X.; Chen, J.; Yan, B.; Zhang, W.; Guddat, L. W.; Liu, X.; Rao, Z. Structural basis for the broad substrate specificity of two acyl-CoA dehydrogenases FadE5 from mycobacteria. *Proc. Natl. Acad. Sci. U. S. A.* **2020**, *117*, 16324–16332.

(65) Minnikin, D. E.; Kremer, L.; Dover, L. G.; Besra, G. S. The methyl-branched fortifications of *Mycobacterium tuberculosis*. *Chem. Biol.* **2002**, *9*, 545–553.

(66) Takayama, K.; Wang, C.; Besra, G. S. Pathway to synthesis and processing of mycolic acids in *Mycobacterium tuberculosis*. *Clin. Microbiol. Rev.* **2005**, *18*, 81–101.

(67) Bhatt, A.; Molle, V.; Besra, G. S.; Jacobs, W. R., Jr.; Kremer, L. The *Mycobacterium tuberculosis* FAS-II condensing enzymes: their role in mycolic acid biosynthesis, acid-fastness, pathogenesis and in future drug development. *Mol. Microbiol.* **2007**, *64*, 1442–1454.

(68) Nataraj, V.; Varela, C.; Javid, A.; Singh, A.; Besra, G. S.; Bhatt, A. Mycolic acids: deciphering and targeting the Achilles' heel of the tubercle bacillus. *Mol. Microbiol.* **2015**, *98*, 7–16.

(69) Gavalda, S.; Léger, M.; van der Rest, B.; Stella, A.; Bardou, F.; Montrozier, H.; Chalut, C.; Burlet-Schiltz, O.; Marrakchi, H.; Daffé, M.; Quémard, A. The Pks13/FadD32 crosstalk for the biosynthesis of mycolic acids in *Mycobacterium tuberculosis*. *J. Biol. Chem.* **2009**, *284*, 19255–19264.

(70) Li, W.; Gu, S.; Fleming, J.; Bi, L. Crystal structure of FadD32, an enzyme essential for mycolic acid biosynthesis in mycobacteria. *Sci. Rep.* **2015**, *5*, 15493.

(71) Bhatt, A.; Molle, V.; Besra, G. S.; Jacobs, W. R., Jr.; Kremer, L. The *Mycobacterium tuberculosis* FAS-II condensing enzymes: their role in mycolic acid biosynthesis, acid-fastness, pathogenesis and in future drug development. *Mol. Microbiol.* **2007**, *64*, 1442–1454.

(72) Gande, R.; Gibson, K. J. C.; Brown, A. K.; Krumbach, K.; Dover, L. G.; Sahm, H.; Shioyama, S.; Oikawa, T.; Besra, G. S.; Eggeling, L. Acyl-CoA Carboxylases (accD2 and accD3), Together with a Unique Polyketide Synthase (Cg-pks), Are Key to Mycolic Acid Biosynthesis in Corynebacteriaceae Such as *Corynebacterium glutamicum* and *Mycobacterium tuberculosis*. *J. Biol. Chem.* **2004**, *279*, 44847–44857.

(73) Sirakova, T. D.; Deb, C.; Daniel, J.; Singh, H. D.; Maamar, H.; Dubey, V. S.; Kolattukudy, P. E. Wax ester synthesis is required for *Mycobacterium tuberculosis* to enter in vitro dormancy. *PLoS One* **2012**, *7*, No. e51641.

(74) Liu, X.; Feng, Z.; Harris, N. B.; Cirillo, J. D.; Bercovier, H.; Barletta, R. G. Identification of a secreted superoxide dismutase in *Mycobacterium avium* ssp. *paratuberculosis*. *FEMS Microbiol. Lett.* **2001**, *202*, 233–238.

(75) Kuhn, M. L.; Alexander, E.; Minasov, G.; Page, H. J.; Warwzrak, Z.; Shuvalova, L.; Flores, K. J.; Wilson, D. J.; Shi, C.; Aldrich, C. C.; Anderson, W. F. Structure of the Essential Mtb FadD32 Enzyme: A Promising Drug Target for Treating Tuberculosis. *ACS Infect. Dis.* **2016**, *2*, 579–591.

(76) DeJesus, M. A.; Gerrick, E. R.; Xu, W.; Park, S. W.; Long, J. E.; Boutte, C. C.; Rubin, E. J.; Schnappinger, D.; Ehrt, S.; Fortune, S. M.; Sasseti, C. M.; Ioerger, T. R. Comprehensive Essentiality Analysis of the *Mycobacterium tuberculosis* Genome via Saturating Transposon Mutagenesis. *mBio* **2017**, *8*, No. e02133.

(77) Dragset, M. S.; Ioerger, T. R.; Zhang, Y. J.; Mærk, M.; Ginbot, Z.; Sacchetti, J. C.; Flo, T. H.; Rubin, E. J.; Steigedal, M. Genome-wide Phenotypic Profiling Identifies and Categorizes Genes Required for *Mycobacterium tuberculosis* Low Iron Fitness. *Sci. Rep.* **2019**, *9*, 11394.

(78) Vadwai, V.; Ajbani, K.; Jose, M.; Vineeth, V. P.; Nikam, C.; Deshmukh, M.; Shetty, A.; Soman, R.; Rodrigues, C. Can inhA mutation predict ethionamide resistance? [Short communication]. *Int. J. Tuberc. Lung Dis.* **2013**, *17*, 129–130.

(79) Liu, K.; Enns, B.; Evans, B.; Wang, N.; Shang, X.; Sittiwong, W.; Dussault, P. H.; Guo, J. A genetically encoded cyclobutene probe for labelling of live cells. *Chem. Commun.* **2017**, *53*, 10604–10607.

## Recommended by ACS

### Cannabichromene and $\Delta^9$ -Tetrahydrocannabinolic Acid Identified as Lactate Dehydrogenase-A Inhibitors by *in Silico* and *In Vitro* Screening

Lewis J. Martin, Lyndsey L. Anderson, *et al.*

APRIL 22, 2021  
JOURNAL OF NATURAL PRODUCTS

READ 

### Unnarmicin D, an Anti-inflammatory Cyanobacterial Metabolite with $\delta$ and $\mu$ Opioid Binding Activity Discovered via a Pipeline Approach Designed to Target Neurotherape...

Riley D. Kirk, Matthew J. Bertin, *et al.*

DECEMBER 07, 2020  
ACS CHEMICAL NEUROSCIENCE

READ 

### A Chiral $^{19}\text{F}$ NMR Reporter of Foldamer Conformation in Bilayers

Siyuan Wang, Simon J. Webb, *et al.*

NOVEMBER 15, 2022  
JOURNAL OF THE AMERICAN CHEMICAL SOCIETY

READ 

### Urea-Bond Scission Induced by Therapeutic Ultrasound for Biofunctional Molecule Release

Yunkang Tong, Xiaojun Peng, *et al.*

SEPTEMBER 07, 2022  
JOURNAL OF THE AMERICAN CHEMICAL SOCIETY

READ 

Get More Suggestions >